Evaluation of WRF Mesoscale Model Simulations of Surface Wind over Iceland

Nikolai Nawri
Guðrún Nína Petersen
Halldór Björnsson
Kristján Jónasson

Veðurstofa Íslands

Evaluation of WRF Mesoscale Model Simulations of Surface Wind over Iceland

Nikolai Nawri, Icelandic Met Office
Guðrún Nína Petersen, Icelandic Met Office
Halldór Björnsson, Icelandic Met Office
Kristján Jónasson, University of Iceland

Keypage

Veðurstofa Íslands

Report no.: VÍ 2012-010	Date: September 2012	ISSN: 1670-8261	Public ☒ Restricted ☐ Provision:

Report title / including subtitle	No. of copies: 20
Evaluation of WRF Mesoscale Model Simulations of Surface Wind over Iceland	Pages: 44
	Managing director: Jórunn Harðardóttir

Authors: Nikolai Nawri Guðrún Nína Petersen Halldór Björnsson Kristján Jónasson	Project manager: Halldór Björnsson
	Project number: 5813-0-0004

Project phase:	Case number: 2012-333

Report contracted for:

IceWind Project

Prepared in cooperation with:

Summary:
In this study, the performance of a particular setup of the Weather Research and Forecasting (WRF) Model with regard to the surface wind conditions over Iceland is analysed, in comparison with local and interpolated station data. Significant and systematic differences exist between model fields and interpolated measurements, with too strong surface winds along the coast, and too weak winds in the interior. The relative decrease in wind speed from the coast inland and onto the higher terrain is further enhanced by about a factor of two for weak geostrophic winds. Qualitatively, throughout most of the island, the WRF model captures the change in mean monthly flow from predominantly offshore in winter, to predominantly onshore in summer, which is shown by the interpolated measurements.

Keywords: Surface wind speed and direction, effects of large-scale circulation, numerical mesoscale model performance, weather research and forecasting model, station data, gridded surface measurements, Iceland	Managing director's signature:
	Project manager's signature:
	Reviewed by:

3

Contents

List of Figures

1 Introduction

In this study, the performance of a particular setup of the Weather Research and Forecasting (WRF) Model with regard to the surface wind conditions over Iceland is analysed, in comparison with local and interpolated station data. Previously, the climatological surface wind conditions at various station locations in Iceland were analysed in Nawri et al. (2012c), while empirical terrain models for surface wind based on Icelandic station data were developed in Nawri et al. (2012a). As the two previous studies, the analysis presented here was conducted in the context of the project "Improved Forecast of Wind, Waves and Icing" (IceWind), Work Package 2, with the ultimate goal of developing a wind atlas for Iceland, primarily for the assessment of wind energy potential.

A special emphasis in this analysis is the influence of complex terrain on the accuracy of the WRF model in reproducing the measured surface wind conditions, and the identification of systematic regional biases. Other topics are the model representation of temporal variability on different time-scales, and the dependence of simulated wind speed on different large-scale overlying flow conditions. The statistical correction of WRF model data based on these comparisons against measurements is discussed in Nawri et al. (2012b).

2 Data

The primary data source for the wind atlas are mesoscale model runs, produced by Reiknistofu í veðurfræði in the context of "Reikningar á veðri" (RÁV), which is a joint project of several Icelandic research institutions. The RÁV model runs were produced with the Weather Research and Forecasting (WRF) Model (Version 3.1.1; see Skamarock et al. (2008) for details). Simulations were performed in three nested horizontal domains, all approximately centred around Iceland: the outer domain with 43×42 grid points spaced at 27 km (1134×1107 km), the intermediate domain with 95×90 grid points spaced at 9 km, and the inner domain with 196×148 grid points spaced at 3 km. The northwest corner of the outer domain covers a part of the southeast coastal region of Greenland. Otherwise, the only landmass included in the model domain is Iceland. For a detailed description of the simulations refer to Rögnvaldsson et al. (2007, 2011a). The data used in this study is that of the inner domain (see Figure 1). Output fields were produced every 3 hours. Data are available for the period 1 Sep 1994 – 2 Nov 2009. However, as described in Nawri et al. (2012c), for comparison with station data, the study period was reduced to the 4 years from 1 Nov 2005 to 31 Oct 2009.

The initial and boundary conditions for the WRF model simulations were determined by 6-hourly operational analyses obtained from the European Centre for Medium-Range Weather Forecasts (ECMWF), valid at 00, 06, 12, and 18 UTC (which is local time in Iceland throughout the year). After initialisation of the model run, these data are only applied at the boundaries, where no observational data are available for comparison. Potential errors in the boundary conditions can therefore not be determined.
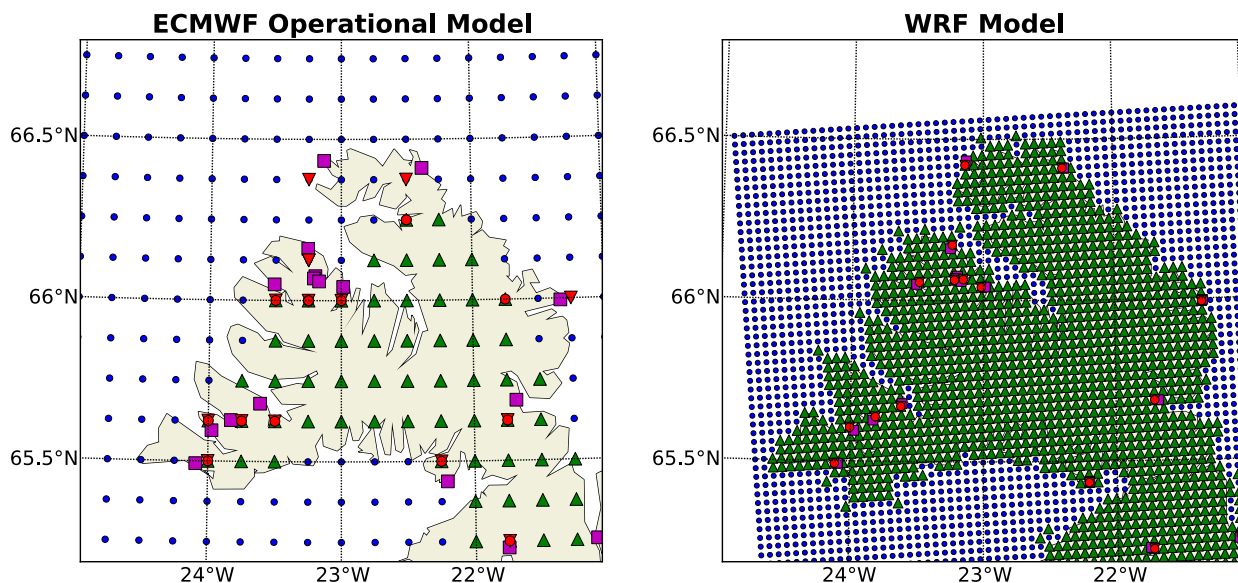
Figure 1. ECMWF and WRF land-sea masks, with ocean grid-points shown by blue dots, and land grid-points shown by green triangles. Also shown are, for each surface weather station (magenta squares), the closest grid-point (red triangles) and the closest land grid-point (red dots).

However, differences of WRF model simulated surface winds from station data can be analysed in relation to corresponding differences from measurements of the operational analyses. For this, both the WRF model fields and operational analyses are interpolated onto station locations. In the case of operational analyses, as discussed in Nawri et al. (2012c), interpolated values are calculated as inverse horizontal distance[1] weighted averages from the four surrounding grid-points. For the WRF model fields, differences between different interpolation methods are insignificant. A mixed method is used, whereby interpolated values are given by inverse distance weighted averages from the four surrounding grid-points, if these grid-points are all over land, according to the model land-sea mask. Along the coast, if any of the surrounding grid-points are over the ocean, the nearest land grid-point value is used at the station location. As shown in Figure 1, the distinction between nearest and nearest land grid-point are only important for the operational analyses, where the nearest land grid-point in regions with a complex coastlines, such as in the Westfjords, can be several kilometres away from a given station location. Interpolated surface wind speed at station locations always refers here to interpolated values from the horizontal field of wind speed, rather than the speed of interpolated wind vectors. Similarly, unless stated explicitly otherwise, for all averages employed throughout the study, mean speed invariably refers to the average of individual speed values, rather than the speed of the averaged wind vector.

In addition to horizontal surface wind, operational analyses of geopotential height at 850 hPa are used to determine the dependence of surface wind conditions over Iceland on the large-scale atmospheric circulation. The angular grid-spacing of these fields is 0.250 degrees in longitude, and 0.125 degrees in latitude, corresponding to a physical grid-spacing of 13.9 km in latitude, and 11.7 km in longitude, along 65°N (see Figure 1). The 6-hourly fields are linearly interpolated onto the 3-hourly times of the observational data.

---

[1]All horizontal distances in this study are calculated along great circles on a spherical Earth at mean sea level.

Quality controlled hourly surface measurements of wind speed and direction, as well as air temperature, were obtained from the Icelandic Meteorological Office. Winds are measured at different heights, h, above ground level (AGL), varying between 4.0 and 18.3 m. These differences are taken into account following WMO guidelines (WMO, 2008), whereby wind speeds are projected to 10 mAGL by

$$S(10\text{m}) = S(h) \frac{\ln(10/z_0)}{\ln(h/z_0)} \ , \tag{1}$$

where for Iceland the surface roughness length z_0 over land is approximately 3 cm (Troen and Petersen, 1989). WRF model surface wind speeds are also valid at 10 mAGL. As described in Nawri et al. (2012c), for any given variable, only those locations are considered, for which station records have at least 75% valid data within any specific period under consideration. The names, ID numbers, and coordinates of all stations from which data was used are given in Nawri et al. (2012c). To be consistent with the WRF model data, the hourly observational time-series were reduced to 3-hourly values.

To relate the spatial variability of surface variables to terrain characteristics, a digital terrain model (DTM) at a 100×100 m resolution was used. This DTM was produced in 2004 by the Icelandic Meteorological Office, the National Land Survey of Iceland (Landmælingar Íslands), the Science Institute of the University of Iceland (Raunvísindastofnun Háskólans), and the National Energy Authority (Orkustofnun).

For the calculation of the shortest distances from station locations and WRF grid-points to the coast, coastline data from the National Geophysical Data Center (NGDC) of the U. S. National Oceanic and Atmospheric Administration were used.

3   Terrain Effects

Terrain-related model errors are due to inaccurate representations of elevation, ruggedness, and surface roughness.

With complex terrain, as exists throughout Iceland, the representation of coastlines and orography greatly depends on spatial resolution. The WRF model elevation on the 3-km grid, in comparison with the 100-m DTM linearly interpolated onto the WRF grid, is shown in Figure 2. Due to the 30 times higher spatial resolution, the DTM shows many of the smaller valleys and fjords, which are not present in the WRF orography. As a result, differences between WRF and DTM elevation vary between ± 300 m. Due to the strong dependence of wind speed on terrain elevation (Nawri et al., 2012a), for a meaningful comparison of regional wind statistics between different datasets, surface wind speeds must be projected to mean sea level according to the respective model terrain and vertical terrain gradients, whereby for station data, the DTM orography is used. As discussed in Nawri et al. (2012a), monthly averages of measured surface wind speed, from about 6 km inland of the NGDC coastline, tend to follow a linear relationship with terrain elevation. As seen in Figures 3 and 4, this is not the case for ECMWF operational analyses. At low elevations, monthly wind speed decreases with height, as the effects of moving inland away from the coast outweigh the effects from increasing elevation. At about 500 metres above mean sea level (mASL), the
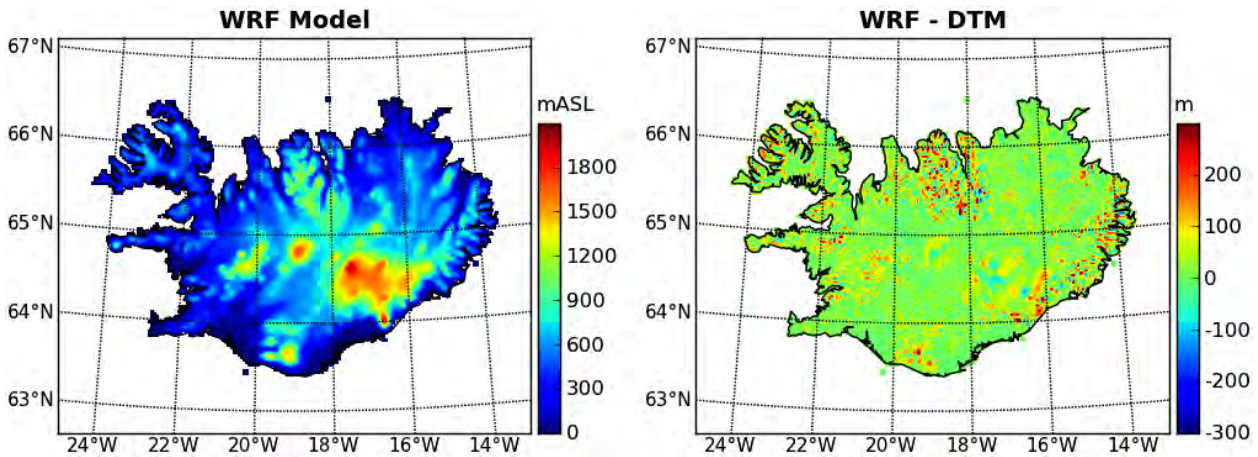
Figure 2. Terrain elevation of the WRF model, and elevation differences between the WRF and the 100-m digital terrain model (DTM), linearly projected onto the WRF model grid.

trend reverses, and wind speed increases with height. The use of linear profiles, as for station measurements, is therefore inappropriate. As shown in the figures, these vertical terrain profiles are better represented by a second order polynomial fit with the square root of height above mean sea level. For measurements, the difference between a linear and second order polynomial fit is negligible. WRF model fields of monthly surface wind speed show a large spread around either a linear or second order polynomial profile. At intermediate elevations, the differences are small. At high elevations, the second order profile provides a better fit, but has too high wind speeds at low elevations, where a larger number of grid-points are located. Therefore, for measurements and WRF model fields, linear profiles are being used, to project surface wind speeds from either the DTM or model orography, respectively, to mean sea level. Throughout the year, the magnitude of vertical terrain gradients determined from WRF model fields is about half that derived from station measurements.

Surface roughness length as specified in the RÁV WRF model setup is shown in Figure 5 for six-months warm and cold seasons. Seasonal differences are due to changes in vegetation and snow cover. Values range from near zero over the permanent icecaps at elevations above 900 mASL, to 50 cm in low-lying areas, which are (for the most part wrongly) identified as being covered with bushes and low trees. In contrast, terrain type throughout Iceland is best described by surface roughness classes 0 to 2, as defined by Troen and Petersen (1989), i.e., by surface roughness lengths of up to 10 cm. Roughness class 3, with roughness lengths of about 40 cm only applies at a few grid-points covering urban and forested areas. Therefore, throughout the year, with the exception of the icecaps, model surface roughness lengths are too large by up to an order of magnitude.

Figure 3. Average January surface wind speeds as a function of terrain elevation for measurements, ECMWF operational analyses, and the WRF model. For operational analyses and the WRF model, all land grid-points over Iceland are used. Red lines represent best linear fits to the monthly data points. Cyan lines represent best second order fits of monthly wind speeds to the square root of terrain elevation.
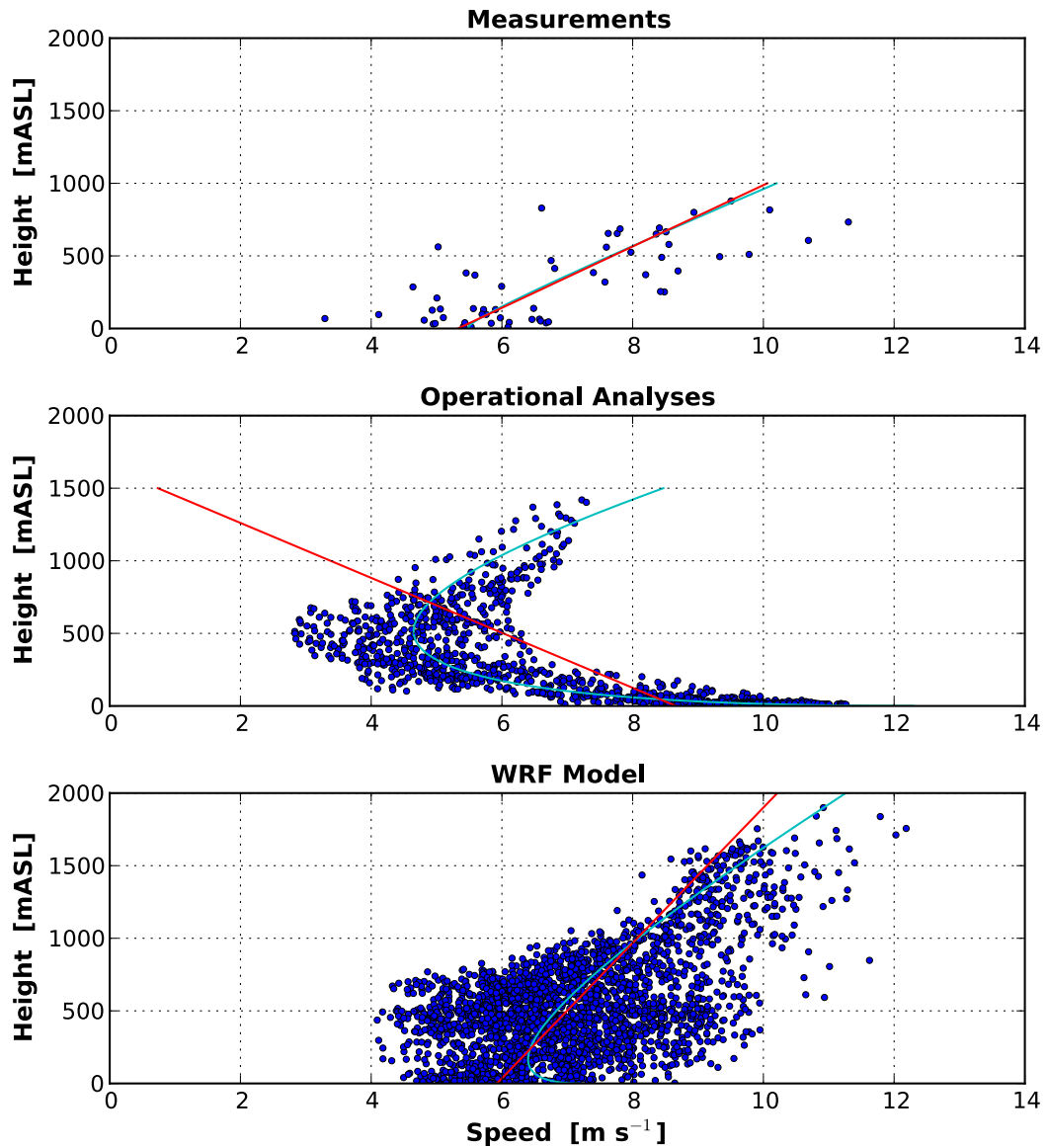
Figure 4. Average July surface wind speeds as a function of terrain elevation for measurements, ECMWF operational analyses, and the WRF model. For operational analyses and the WRF model, all land grid-points over Iceland are used. Red lines represent best linear fits to the monthly data points. Cyan lines represent best second order fits of monthly wind speeds to the square root of terrain elevation.
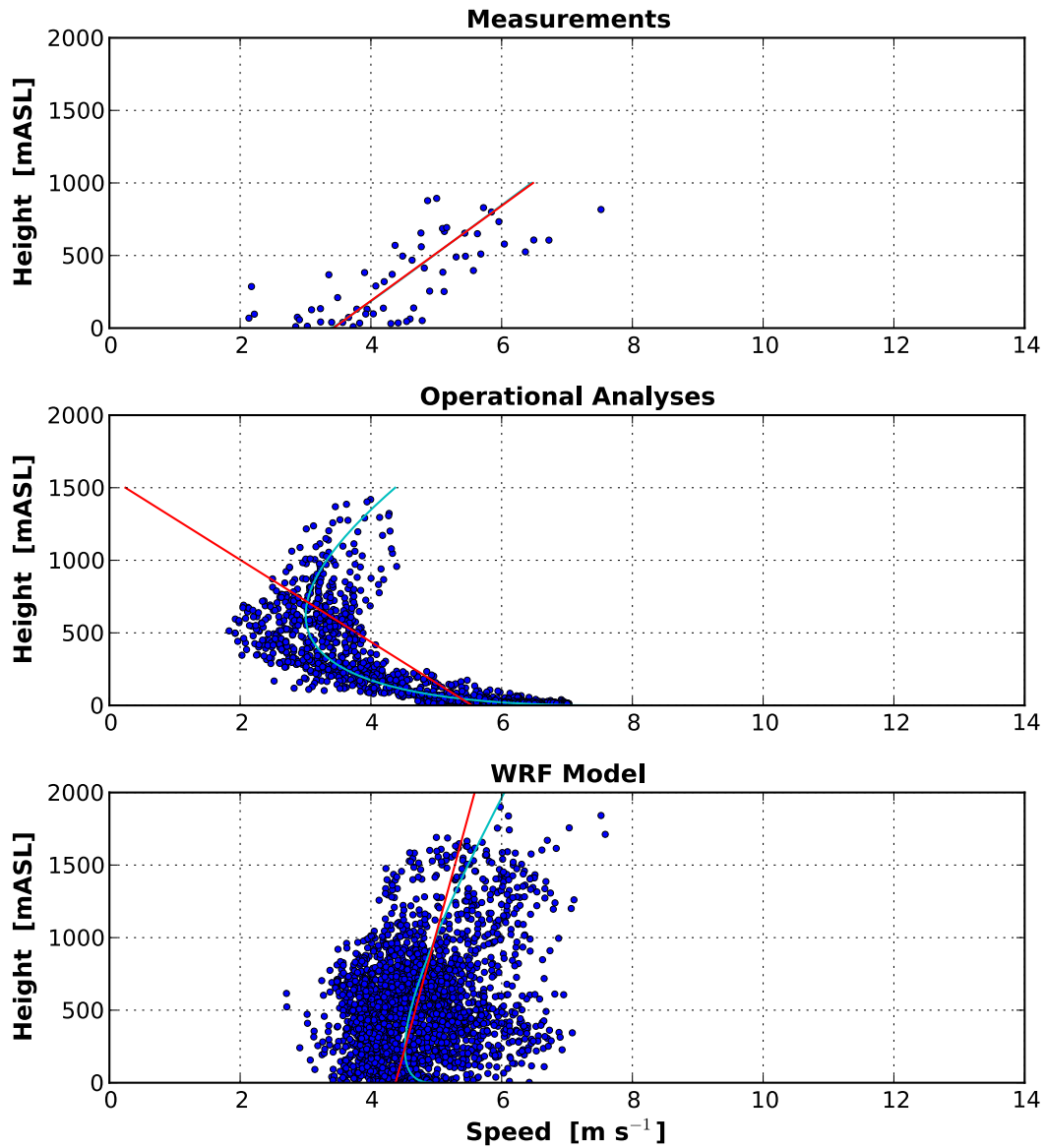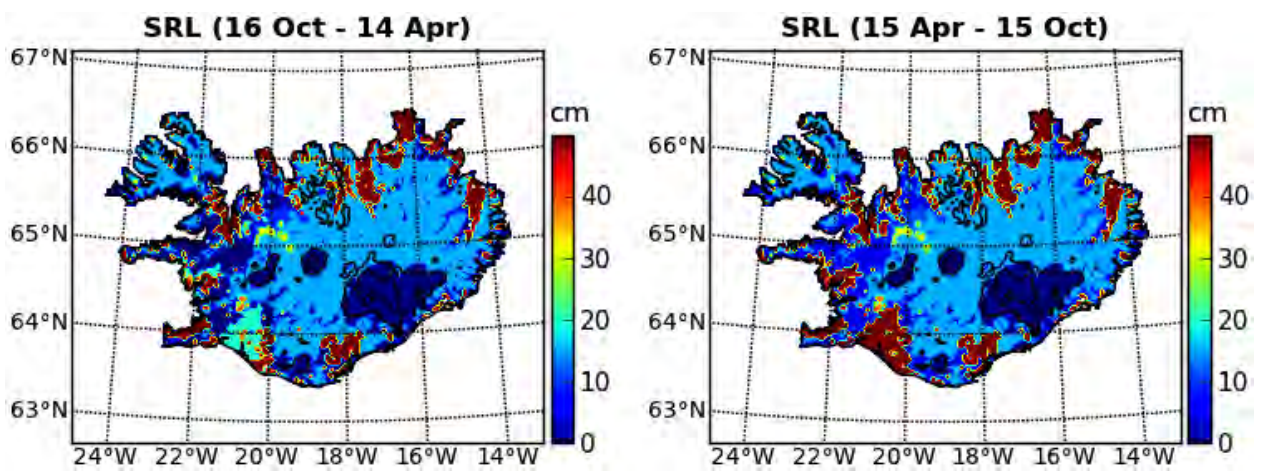
Figure 5. Surface roughness length over the land area of Iceland, as used in the WRF model during the cold and warm season. Terrain elevation contour lines are drawn at 1000 and 1500 mASL.

4 Monthly Mean Fields

Monthly WRF model fields of surface wind speed in January and July, in comparison with the one-parameter empirical terrain model developed in Nawri et al. (2012a), are shown in Figure 6. Throughout the year, significant and systematic differences exist between WRF model fields and interpolated measurements, with too strong model surface winds along the coast, and too weak winds in the interior. The relative decrease in wind speed from the coast inland and onto the higher terrain is due to unrealistically high values of surface roughness lengths in the model, and too small vertical terrain gradients, as discussed in the previous section.

Monthly vector fields of horizontal wind at mean sea level are shown in Figure 7 for the entire island, and in Figure 8 for the Westfjords.[2] As described in more detail in Nawri et al. (2012a), horizontal vector fields at mean sea level are calculated from the projected values of wind speed, with averaged unit vectors calculated from the original wind directions. Qualitatively, throughout most of the island, the WRF model captures the change in mean monthly flow from predominantly offshore in winter, to predominantly onshore in summer, which is shown by the interpolated measurements. However, in summer, the southerly onshore wind component across the southern half of the island is generally underestimated. In winter, differences at many grid points are large, but unsystematic.

focusing more specifically on downslope/offshore and onshore/upslope winds, the seasonal change in the mean monthly inland component of measured and modelled wind vectors at station locations is shown in Figure 9. The inland wind component is calculated by projecting the horizontal wind vector onto the unit vector pointing from the given station location to the point at (18.35°W, 64.77°N), situated between Hofsjökull and Vatnajökull. The seasonal change is defined as the difference between July and January averages. In the eastern and northern part of the island, the local magnitudes of seasonal flow reversal in WRF model simulations are similar to those based on measurements. However, in the southwest region the flow reversal is significantly too weak, partly due to weak wintertime offshore winds, and continued summertime downslope flow from the central highland, as seen in Figure 7.

---

[2]The stereographic projection of wind vectors employed for these figures is described in Nawri et al. (2012c).
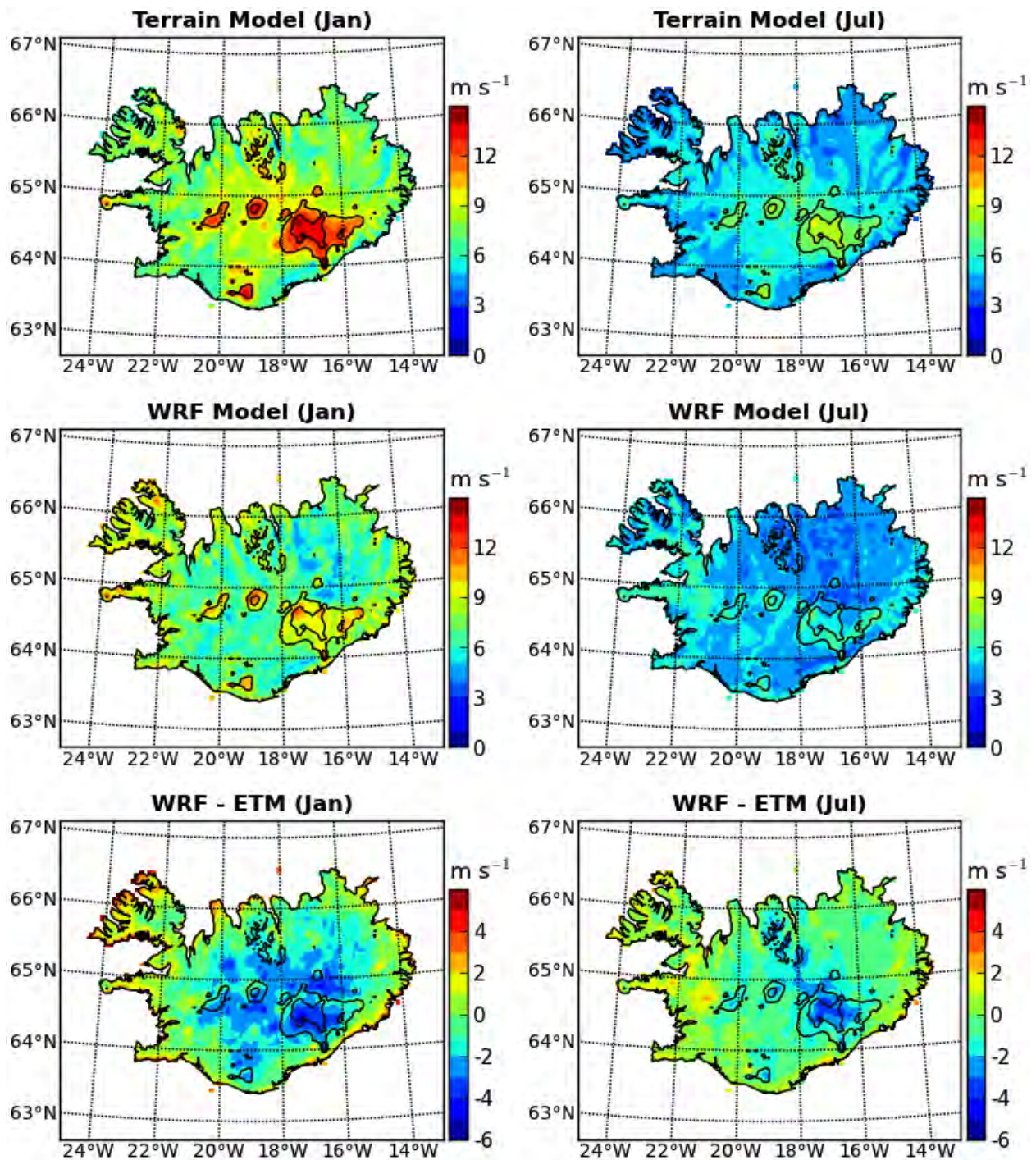
Figure 6. Surface wind speed according to the one-parameter empirical terrain model (ETM) and the WRF model. Terrain elevation contour lines are drawn at 1000 and 1500 mASL.
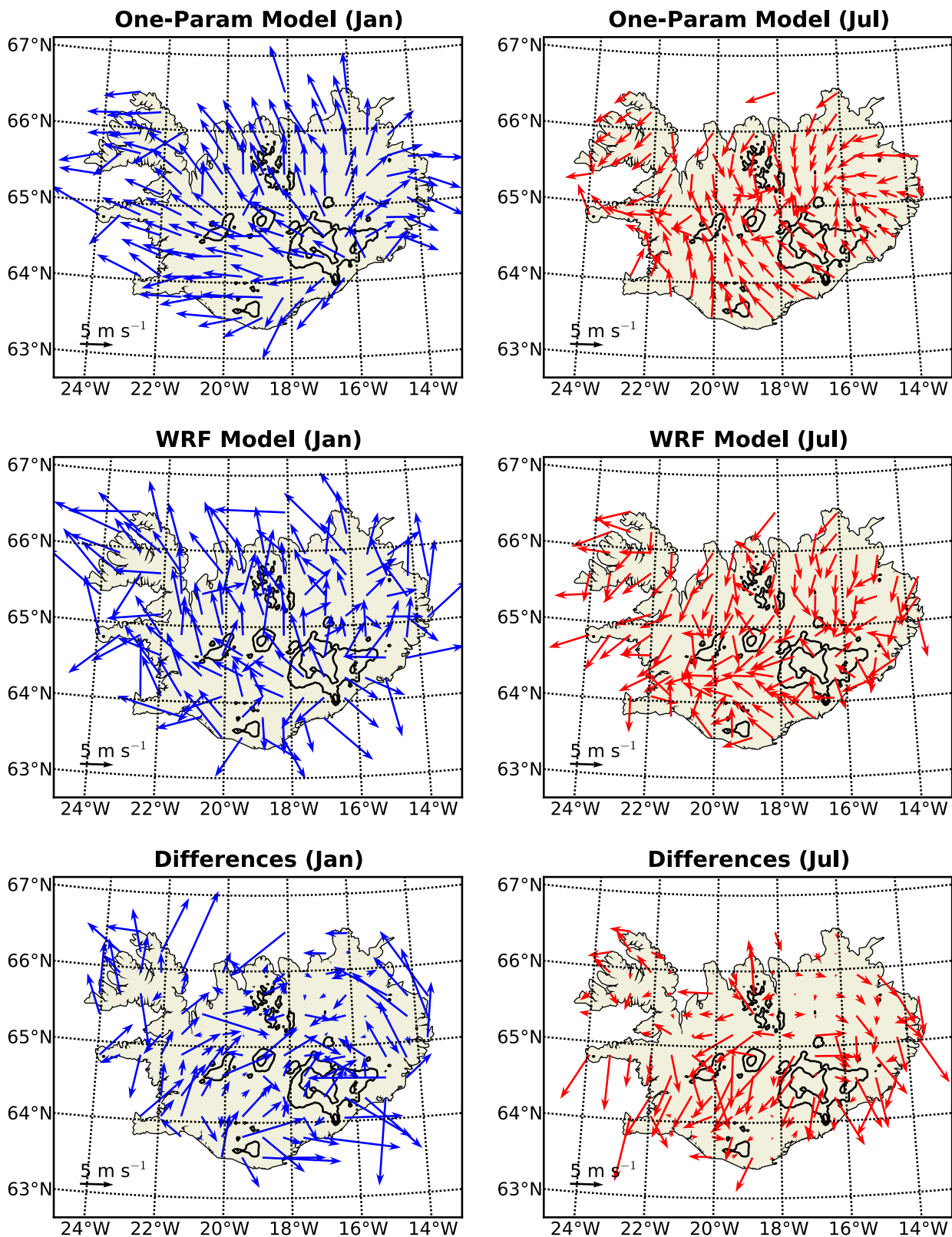
Figure 7. Horizontal wind vectors at mean sea level according to the one-parameter terrain model and the WRF model. Differences are calculated between the WRF and the terrain model.

Figure 8. Horizontal wind vectors at mean sea level in the northwest region of Iceland according to the one-parameter terrain model and the WRF model. Differences are calculated between the WRF and the terrain model.

Figure 9. Seasonal change in the mean monthly inland component of measured and modelled wind vectors at station locations (see Section 4).

5 Seasonal Cycles

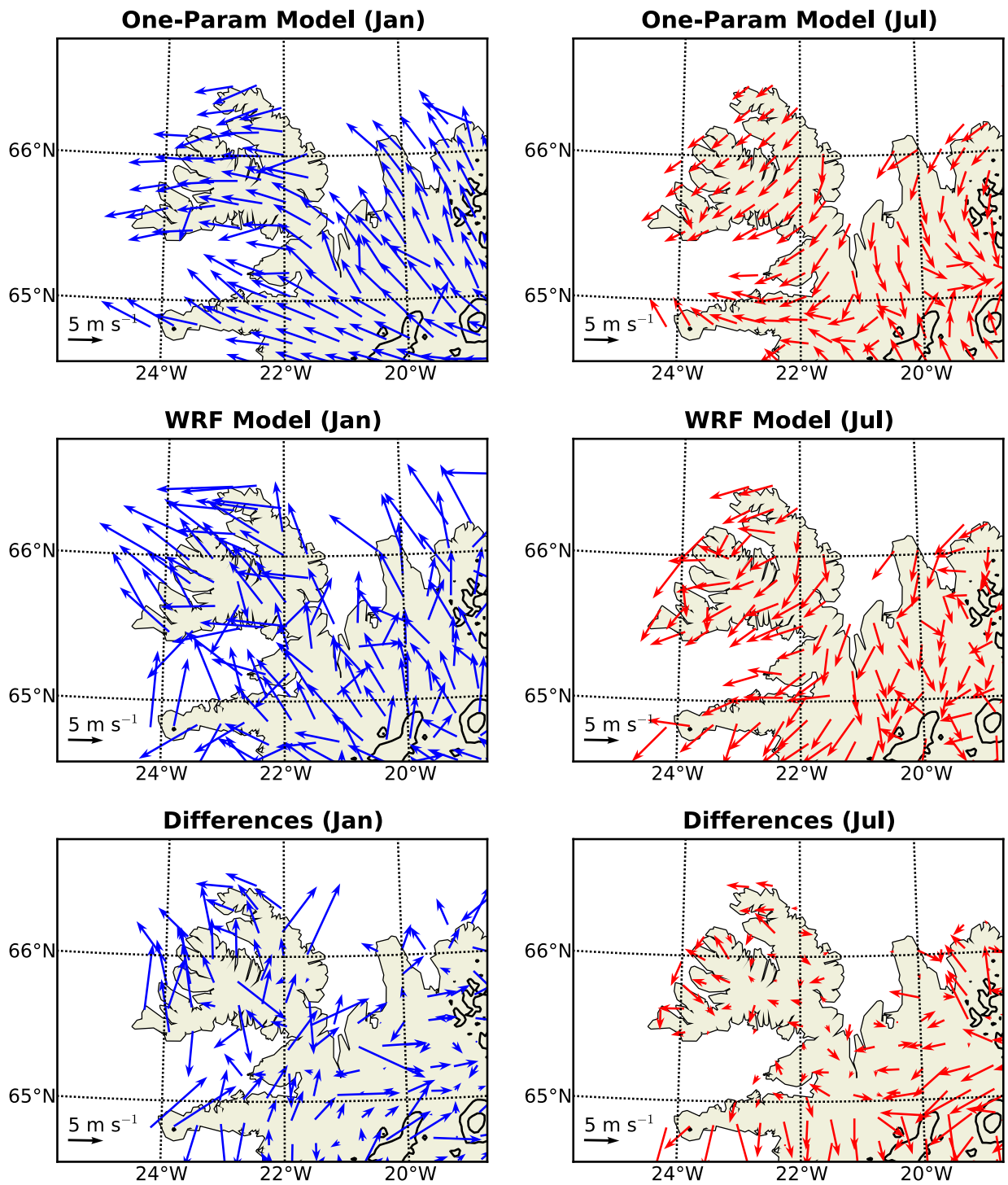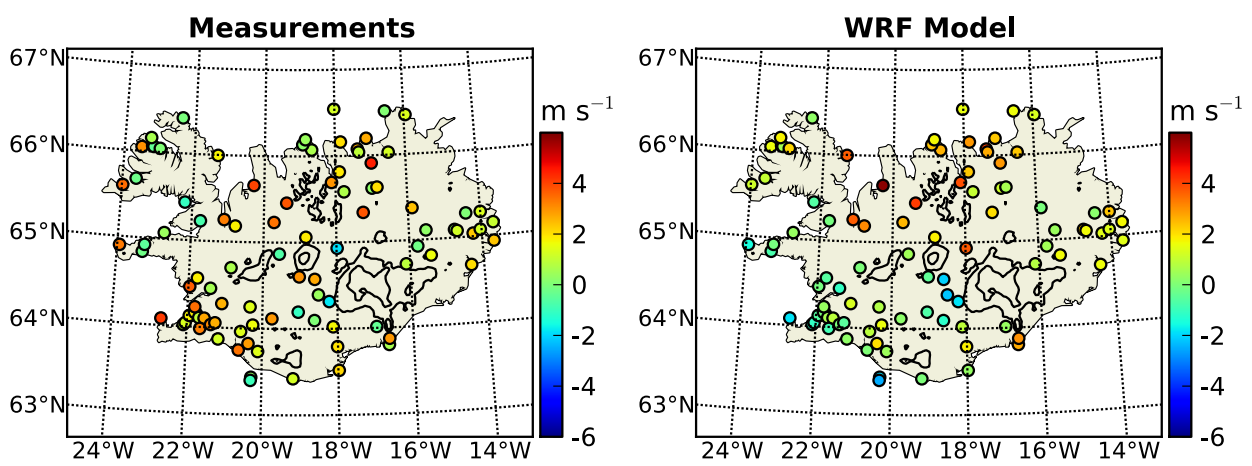Similar to the discussion in Nawri et al. (2012c), for the calculation of seasonal cycle of surface wind speed, stations are separated either by local terrain elevation, or by geographical region.

According to terrain elevation, z_s, stations are classified as

- low coastal for $0 \leq z_s < 15$ m,
- high coastal for $15 \leq z_s < 50$ m,
- intermediate for $50 \leq z_s < 400$ m,
- high for $z_s \geq 400$ m ,

where ECMWF operational analyses and WRF model data are projected to the local terrain elevation, as given by the 100-m DTM. According to longitude, λ_s, and latitude, ϕ_s, stations are classified as belonging to

- the northwest region for $\lambda_s < -18°$E and $\phi_s \geq 65°$N,
- the northeast region for $\lambda_s \geq -18°$E and $\phi_s \geq 65°$N,
- the southwest region for $\lambda_s < -18°$E and $\phi_s < 65°$N,
- the southeast region for $\lambda_s \geq -18°$E and $\phi_s < 65°$N,

where local wind speeds are projected to mean sea level. These definitions differ from those in Nawri et al. (2012c), in that there, operational analyses data was taken at the ECMWF model elevation. Additionally, for the regional comparison, stations were limited to the lowest 50 mASL. The effect of these different definitions is that ECMWF surface wind speeds at low elevations are increased, when projecting to mean sea level, without affecting the relative variation of the seasonal cycles.

Whether separated by elevation or by region, the ensemble mean surface wind speeds in WRF model simulations qualitatively follow the same seasonal cycles as those according to station data and operational analyses. However, compared with the latter two, the WRF seasonal cycles at locations near the coast are overall shifted to higher values by about $1-2$ m s^{-1} (see Figure 10). Contrary to the measured wind speeds, which show consistently higher monthly values at elevations of at least 400 mASL than below, WRF monthly surface wind speeds in the elevated interior are consistently lower than at lower elevations, especially in winter. Based on local values, this was already seen in Section 3.

The regional comparison of seasonal cycles of surface wind speed, projected to mean sea level, is shown in Figure 11. Since in all four quadrants of the island the majority of stations are near the coast, the ensemble mean speeds in the WRF model simulations are consistently higher than those based on station data. The most significant regional difference in WRF model simulations are low cold-season monthly wind speeds in the northeast quadrant compared with those in other regions. This is not the case based on either station data, or operational analyses.

Figure 10. Seasonal cycle of surface wind speed at station locations separated by local terrain elevation: individual station data (dashed black lines), ensemble averages of station data (blue lines), ensemble averages of interpolated operational analyses (green lines), and ensemble averages of interpolated WRF simulations (red lines).

6 Local Differences

In the previous sections, the regional bias in WRF simulations with generally too strong coastal and too weak interior surface wind speeds has been established. In this section, the nature of local deviations in WRF surface wind speeds from measurements is compared with corresponding differences of ECMWF operational analyses.

Histograms of wind speed differences, projected to mean sea level, at four locations in January are shown in Figure 12. As seen previously, mean sea level wind speeds in the operational analyses are generally too high. Their difference distributions are therefore shifted towards higher values compared with the WRF differences. However, the shapes of the difference distributions of WRF and ECMWF surface winds at individual locations are similar, considering the differences between
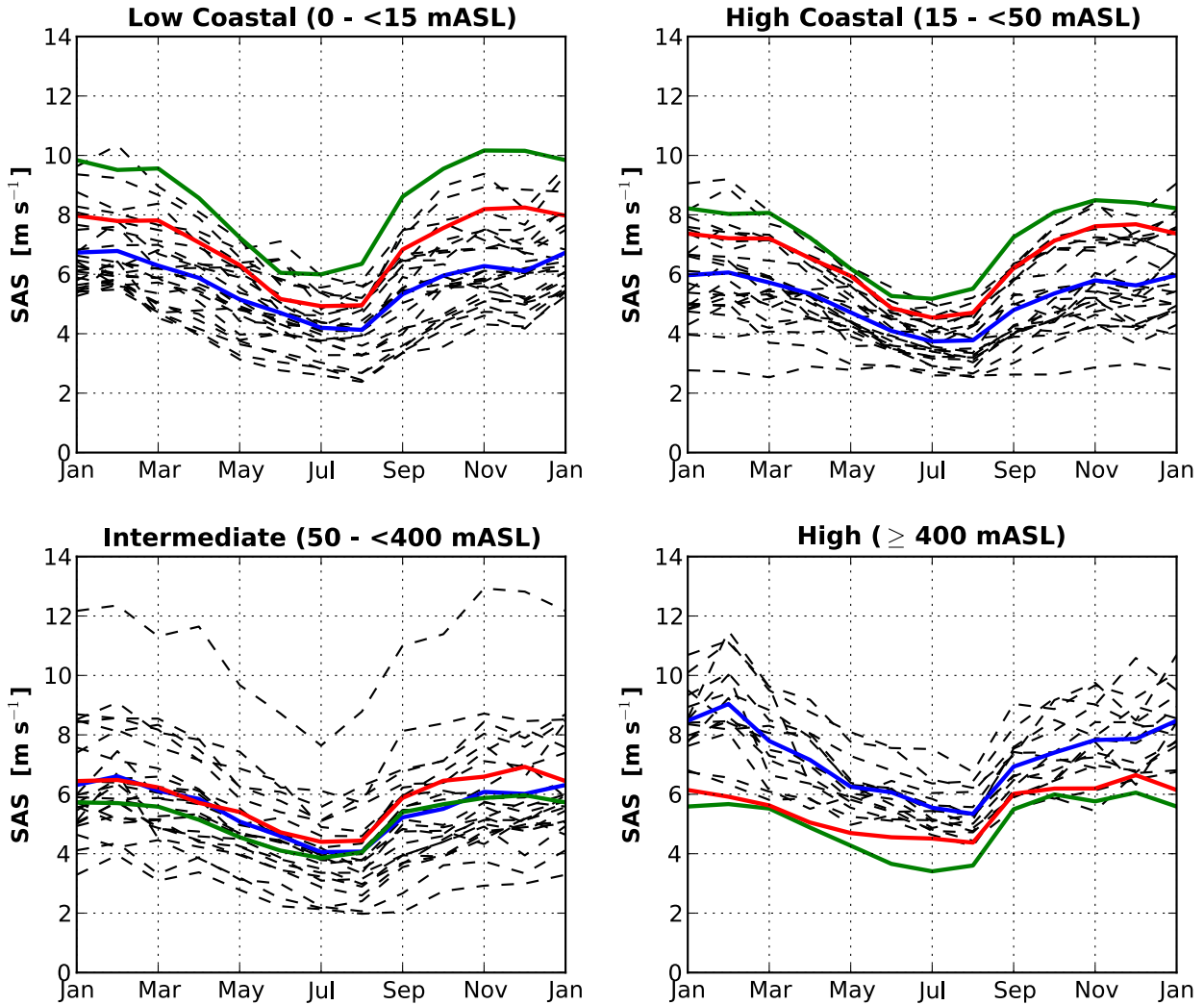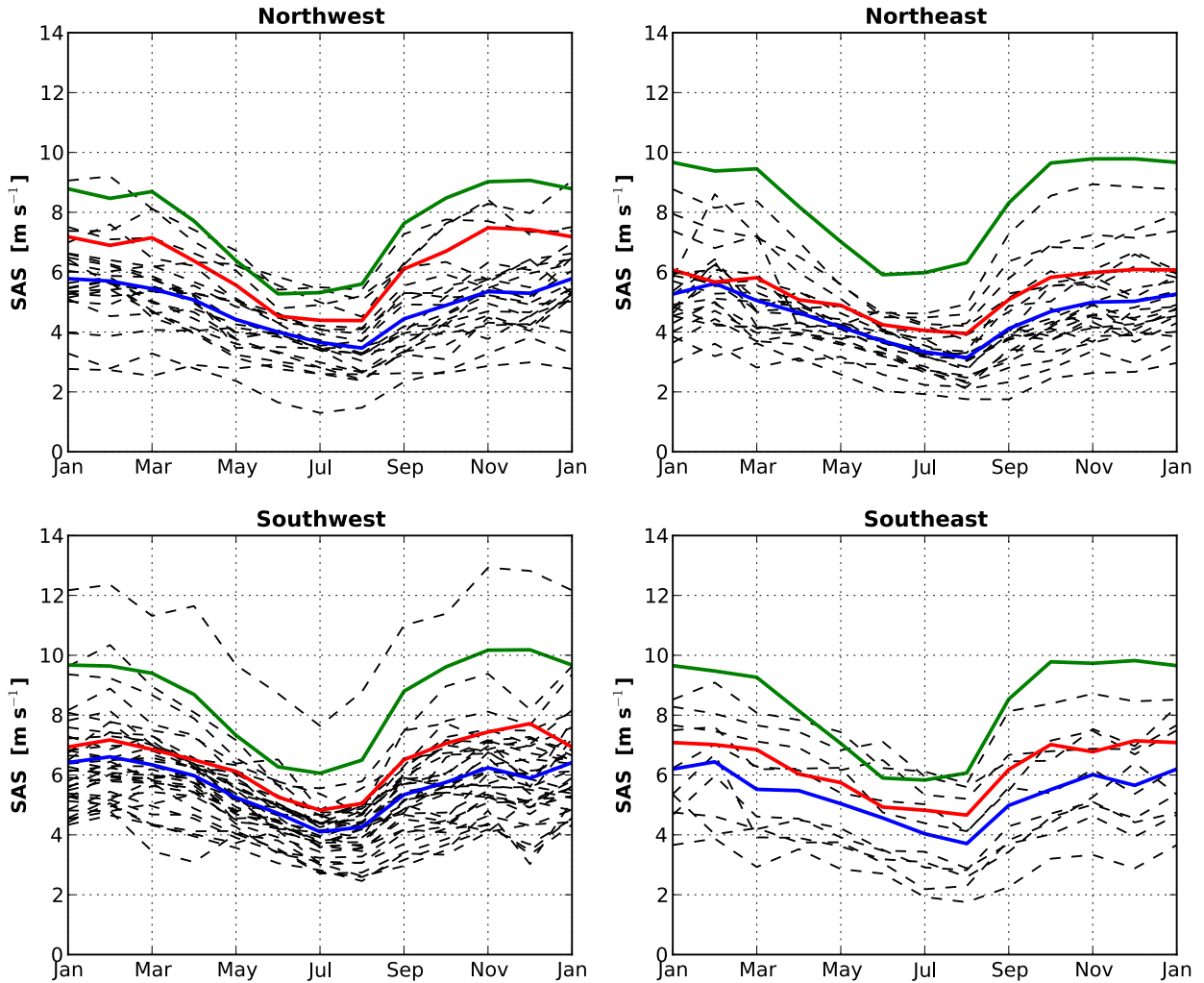
Figure 11. Seasonal cycle of surface wind speed at station locations separated by region: individual station data (dashed black lines), ensemble averages of station data (blue lines), ensemble averages of interpolated operational analyses (green lines), and ensemble averages of interpolated WRF simulations (red lines).

different locations. At all locations, differences are approximately normally distributed, with wider distributions in winter than in summer (not shown). Isafjörður (Station 2642) (see the tables and maps in Nawri et al. (2012c)) is located at low elevations within a narrow fjord, poorly resolved by the WRF model terrain, in the western part of the Westfjords. WRF surface winds there have a small positive bias, with an intermediate spread of differences to measured wind speeds. Very similar difference distributions are found at Reykjavík Airport (Station 1477), located at low elevations at the southwest coast, in a relatively flat but built-up area, with a small wooded region nearby. Hallormsstaður (Station 4060) is located at low elevations within a poorly resolved, densely wooded river valley, about 60 km from the open east coast. WRF surface winds there show a positive bias of about 3 m s^{-1}, with a relatively small spread of the difference distribution. Þúfuver (Station 6760) is located at intermediate elevations within relatively flat and open terrain in the interior of the island. As seen in the previous sections, WRF winds in that region are generally too weak, resulting in a large negative bias of about -5 m s^{-1}, and a wide difference distribution.
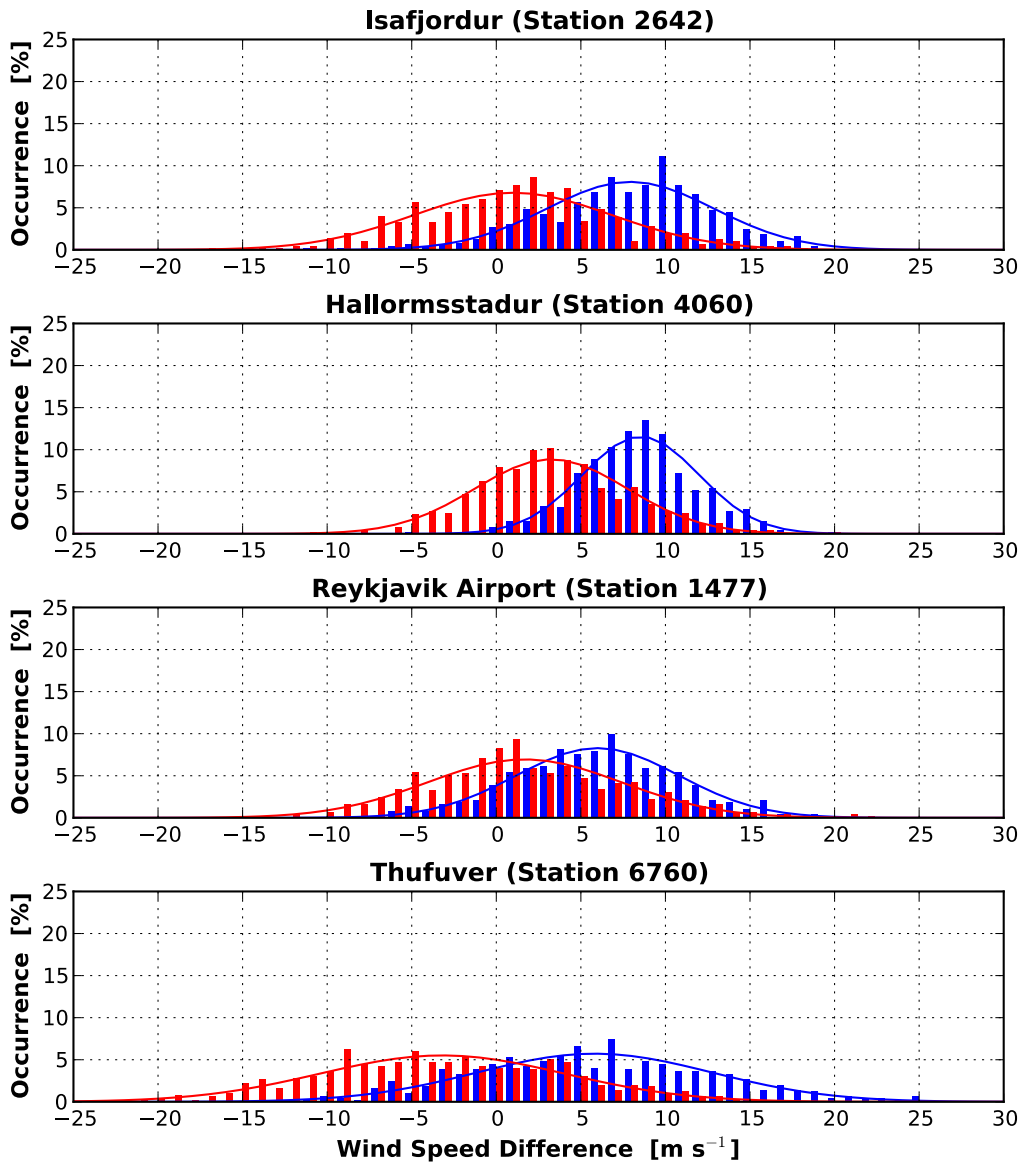
Figure 12. Histograms of differences between modelled and measured surface wind speeds, projected to mean sea level, in January: ECMWF operational analyses (blue bars), and WRF model (red bars). The lines indicate normal distributions with the standard deviations of the actual distributions.

Based on these four stations alone, it is clear that significant differences exist at different locations in the distribution of deviations of either WRF or ECMWF winds from measurements. However, since differences are approximately normally distributed, the nature of deviations of modelled or analysed surface winds from measurements can easily be compared at all locations across the island. The two parameters that determine local normal distributions are the monthly average difference, and the half-width, $2\sqrt{2\ln 2}\sigma$, which is proportional to the monthly standard deviation of differences, σ.
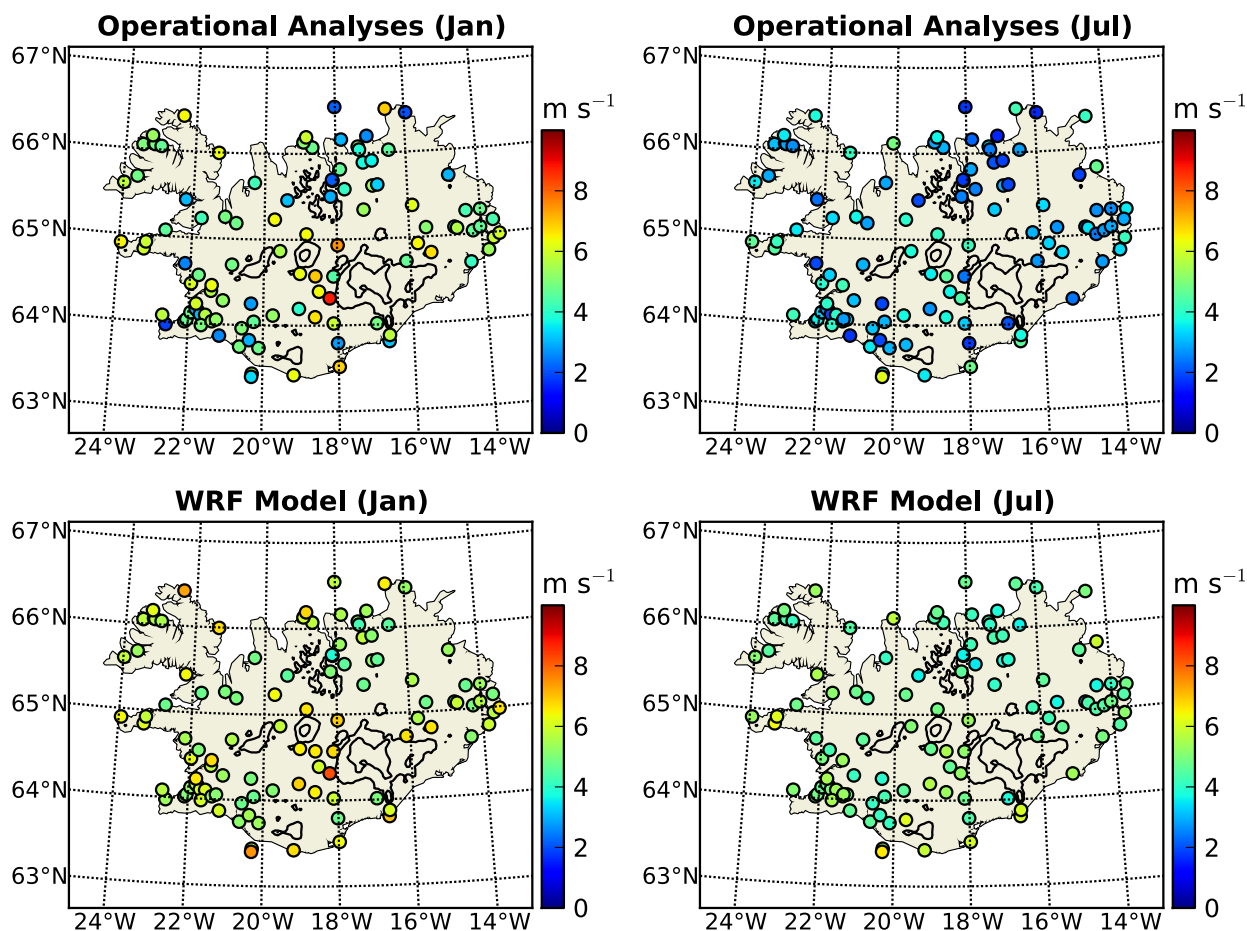
Figure 13. Standard deviation of differences between modelled and measured surface wind speeds, projected to mean sea level.

Monthly biases of WRF surface wind speeds have already been discussed in connection with Figure 6. The local values of standard deviations are shown in Figure 13. The similarity between the standard deviations of differences from measurements of WRF and ECMWF winds, which was seen at the four locations discussed above, is consistent across the island. As discussed in more detail below, this is the result of a high temporal correlation between WRF and ECMWF surface winds. It will be seen that, despite differences in monthly averages, temporal fluctuations around average values in the WRF model simulations are primarily driven by the boundary conditions.

7   Statistical Differences and Correlations

As seen in the previous section, local differences between either WRF or ECMWF and measured surface wind speeds, projected to mean sea level, are approximately normally distributed. In this section, the statistical differences and similarities between modelled and measured time-series are investigated in more detail.

The linearity of the relationship between observed time-series O_i at the i-th location, and corresponding time-series S_i derived from linearly interpolated model fields, is measured by correlation,

$$C_i = \frac{E\left[(S_i - E[S_i])\,(O_i - E[O_i])\right]}{D[S_i]\,D[O_i]} \;, \tag{2}$$

where averages and standard deviations of any set of values are denoted by $E[\;]$ and $D[\;]$, respectively. Overall absolute differences between observed and modelled time-series can be measured by mean squared deviation (MSD),

$$M_i = E\left[(S_i - O_i)^2\right] \;, \tag{3}$$

with normalised mean squared deviation (NMSD) defined as

$$N_i = \frac{M_i}{D[S_i]\,D[O_i]} \;. \tag{4}$$

Since correlation is an overall measure of the temporal fluctuations around average values for each of the time-series, even with a high correlation, MSD may be large due to a constant offset between the two time-series.

As a combined measure of average biases and differences in variability, an error function,

$$F_i = (E[S_i] - E[O_i])^2 + (D[S_i] - D[O_i])^2 \;, \tag{5}$$

can be defined as the sum of squared differences between averages and standard deviations of measured and modelled time-series. With time-series decomposed into temporal averages and perturbations,

$$S_i = S_i' + E[S_i] \;, \tag{6}$$

it can be shown that

$$F_i = M_i + 2\,\mathrm{cov}(S_i, O_i) - 2\,D[S_i]\,D[O_i] \geq 0 \;. \tag{7}$$

Division by $D[S_i]\,D[O_i]$ leads to

$$N_i \geq 2\,(1 - C_i) \;. \tag{8}$$

For a given correlation, C_i, this relationship establishes a lower bound, $2\,(1 - C_i)$, for NMSD at those locations, at which the error function, F_i, vanishes, i.e., where modelled averages and standard deviations are equal to the measured values. Beyond that value, absolute deviations cannot be reduced without changing the correlation, and thus the temporal variability of modelled time-series.
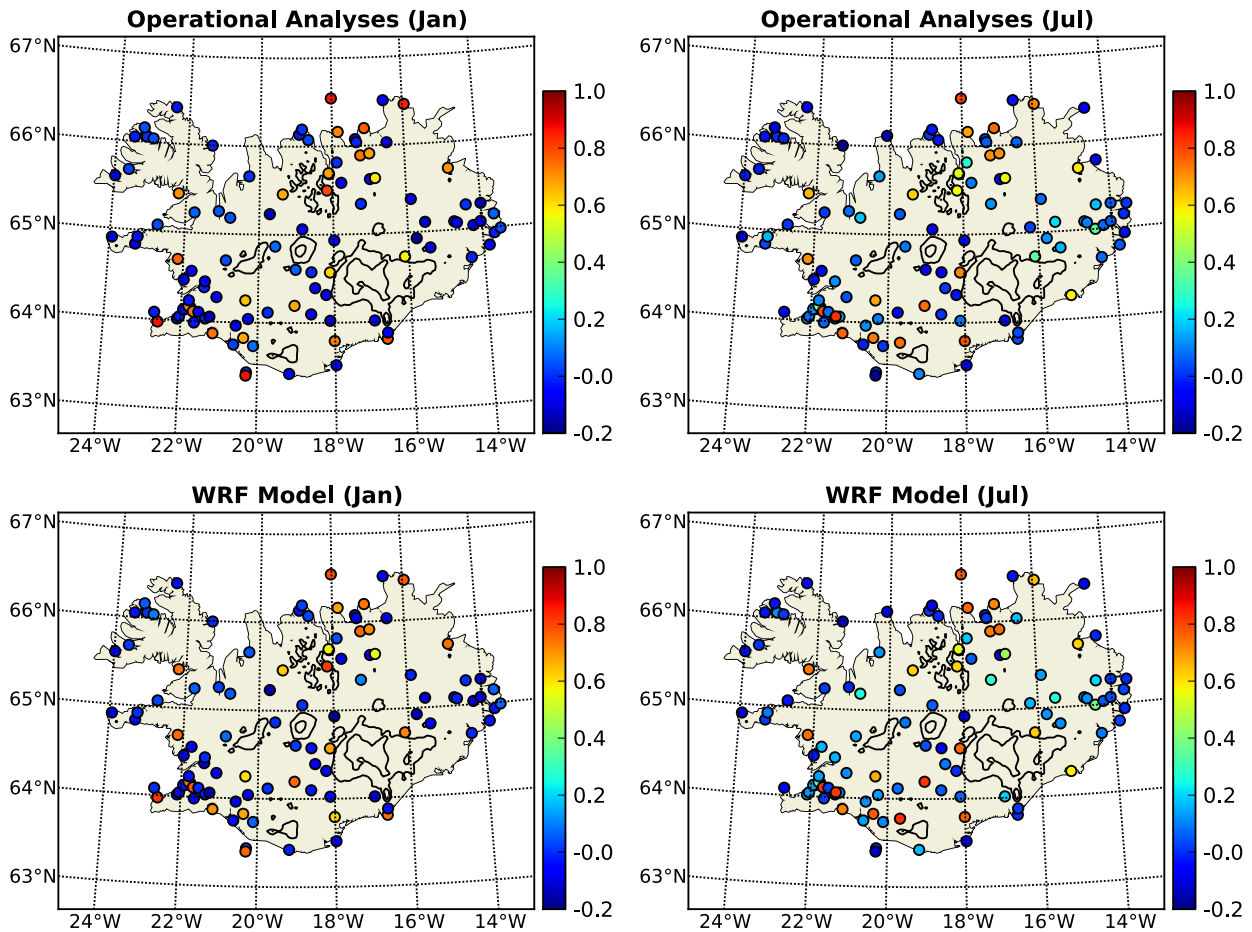
Figure 14. Surface wind speed correlation between measurements and either ECMWF operational analyses or the WRF model.

Local correlations between measured and modelled time-series of surface wind speed are shown in Figure 14. For the most part, there is a clear distinction between high- and low-correlation sites, without significant differences between different years (not shown). However, especially at low-correlation sites, correlation tends to be higher in summer than in winter. Compared with the large differences in correlation between nearby locations, differences between WRF and ECMWF correlations with measured wind speeds are small.

In fact, as shown in Figure 15, WRF surface wind speeds, especially in winter, are highly correlated with those interpolated from ECMWF operational analyses. In summer, at a few locations in the interior, correlations fall below 0.6, but generally remain above that value. Temporal fluctuations of WRF surface wind speeds, to a large extent, are therefore driven by the 6-hourly boundary conditions, rather than internal model dynamics. However, terrain effects on the temporal variability of the horizontal wind field are noticeable in the reduced correlations of individual vector components. This is particularly the case for the zonal wind component in regions of increased terrain ruggedness.
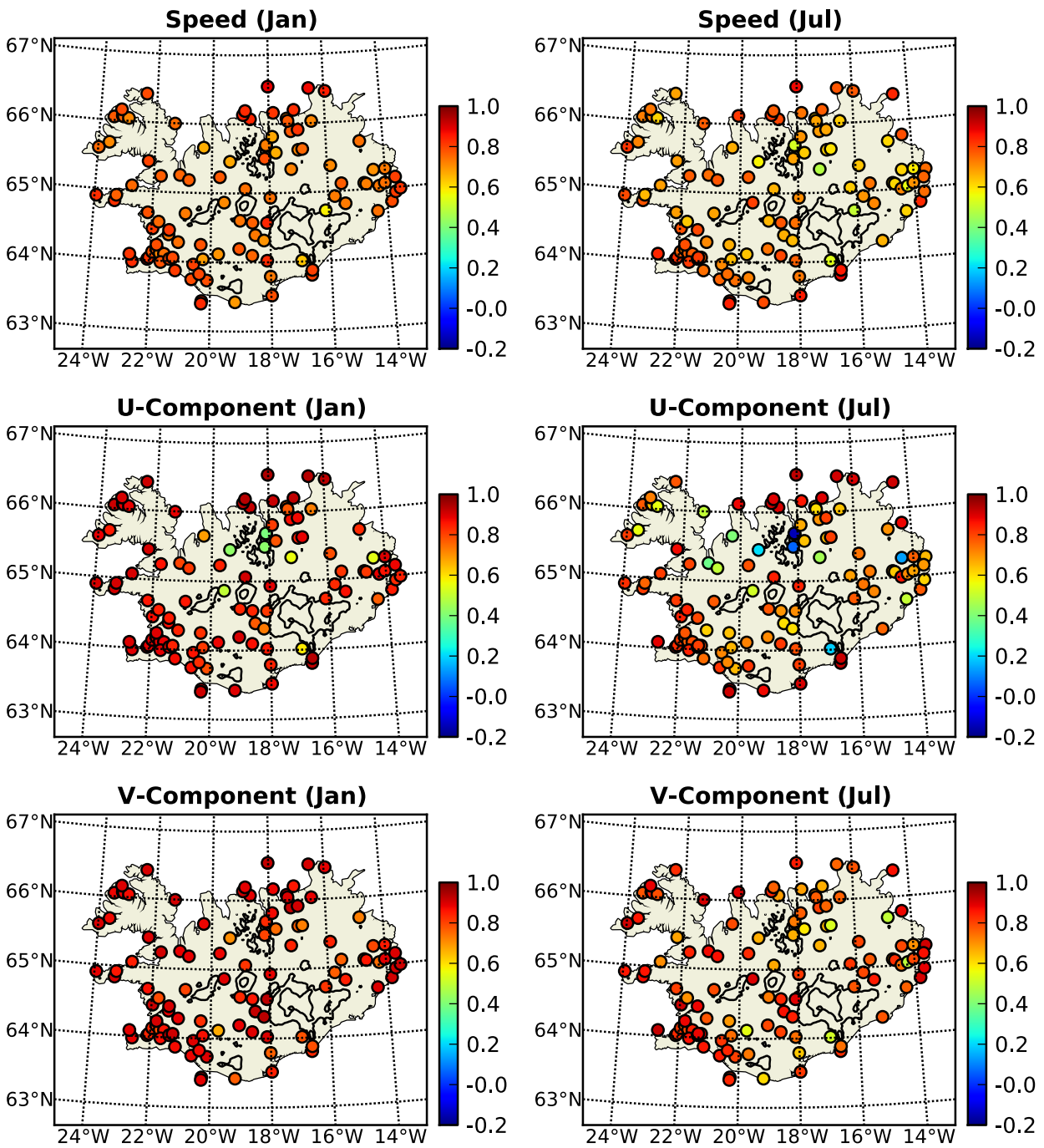
Figure 15. Correlation between ECMWF operational analysis and WRF model surface wind speeds and horizontal velocity components.

Referring again to Figure 14, geographically, for the most part, high- and low-correlation sites are well mixed. However, especially in winter, consistently low correlations are found in the Westfjords and in the central part of the east coast. Correlating overlying ECMWF geostrophic wind speeds at 850 hPa with measured surface wind speeds, the same division into high- and low-correlation sites was found by Nawri et al. (2012a). In that study it was shown that high correlations primarily exist under conditions of strong geostrophic winds. Furthermore, analysing smoothed time-series, it was found that a more consistent response of surface wind speeds across the island towards changes in the intensity of the prevailing overlying flow exists at time-scales of two weeks and longer.

However, even based on the original 3-hourly time-series, it is easy to verify that the dynamics creating temporal fluctuations at low-correlation sites, which are essentially disconnected from those of the geostrophic or actual ECMWF winds, are not purely local. This is done by projecting measured surface wind speeds to mean sea level, using the vertical terrain gradients introduced in Section 3, and calculating the horizontal average at each time-step. Additionally, to identify the connection of temporal fluctuations on different time-scales, the local and horizontally averaged time-series are smoothed by the application of running means over periods from 1 to 30 days. Correlations of the complete four-year time-series of local mean sea level wind speeds with the horizontally averaged wind speed are shown in Figure 16. In general, original 3-hourly time-series at locations, where wind speeds are poorly correlated with ECMWF and WRF winds, are better correlated with the regional average than those at high-correlation sites with respect to ECMWF and WRF winds. This is particularly the case in the Westfjords and in the east, and would be highly unlikely, if local temporal variations were primarily determined by the specific circumstances at each of the individual measurement sites. As important as local forcing mechanisms clearly are, some regional coherence in dynamics and temporal variability of surface wind speed is maintained, which is not captured by the operational analyses, at least at the model boundaries. Correlations between local and regionally averaged wind speeds generally increase if time-series are smoothed by 1-day running means, especially along the coast of the northern half of the island, with average correlation for all stations increasing from 0.390 to 0.418. Since thermal wind systems and atmospheric tides are effectively filtered out by the smoothing, the coherent regional variability of wind speed over Iceland is not predominantly related to diurnal cycles. Local correlations along the northern coast remain high for 3-day running means, but start to decrease slightly in the interior, with an average for all stations of 0.398. With increasing smoothing periods, correlations continue to decrease throughout the island.
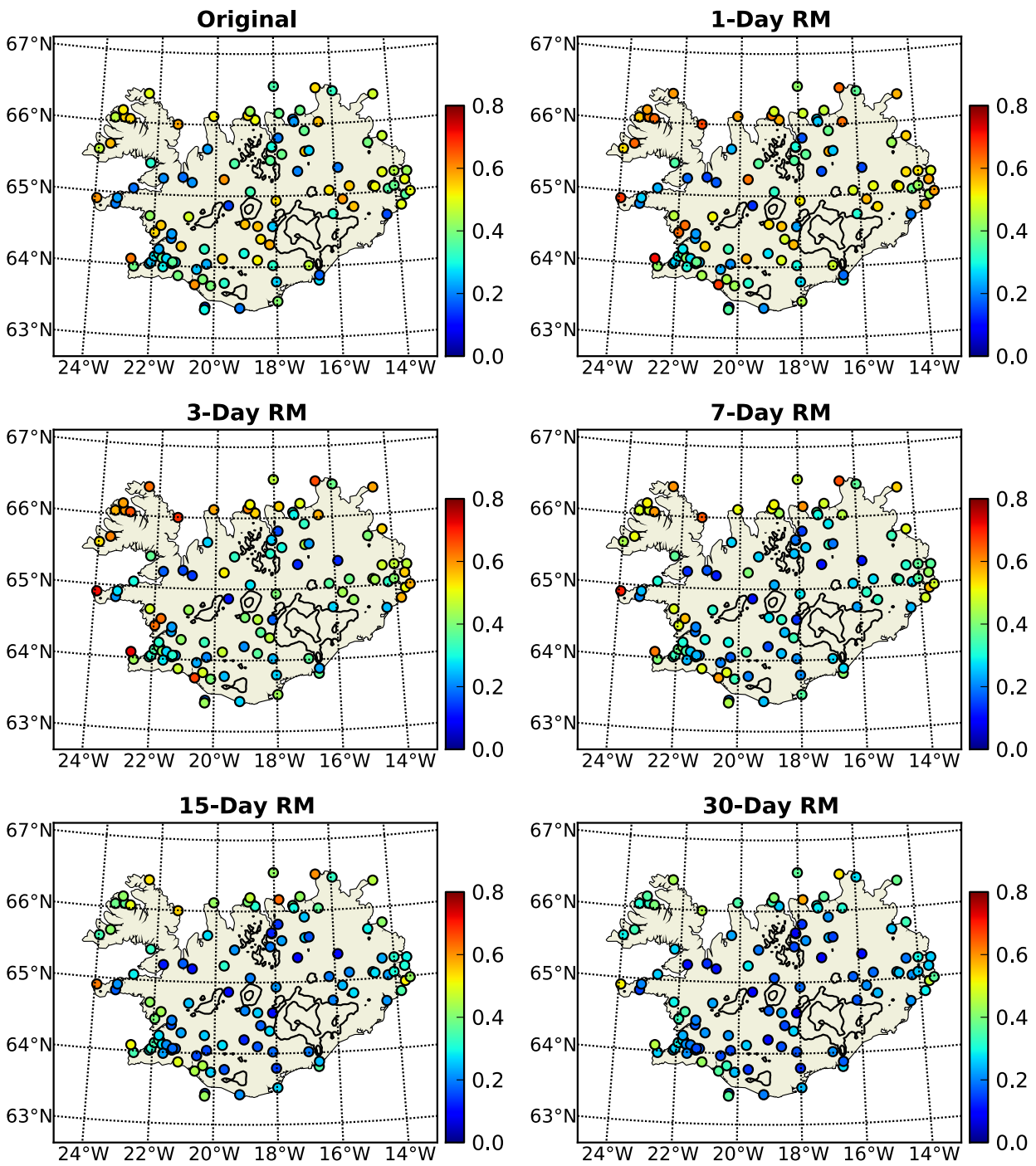
Figure 16. Correlation between local and regionally averaged measured surface wind speeds, with 3-hourly time-series smoothed by running means over different time-periods.

Local correlations between WRF model and measured time-series of surface wind speed, projected to mean sea level and smoothed by running means over periods from 1 to 30 days, are shown in Figure 17. With increasing smoothing period, the differences between low- and high-correlation sites at low elevations and near the coast are reduced, with only small changes in the elevated interior of the island. At 0.244, average correlation for all stations is highest for 3-day running means, but only slightly smaller for 1- and 7-day running means, with values of 0.235 and 0.237, respectively. The dominant weather phenomenon on those time-scales best represented by ECMWF operational analyses at the model boundaries, and subsequently by the WRF model, is the evolution of individual cyclonic weather systems, of which the majority pass south of the island, being associated with the climatological feature of the Icelandic Low (Einarsson, 1984). By contrast, for ECMWF geostrophic wind speeds at 850 hPa and measured surface wind speeds, the highest correlations are found for 15-day running means (Nawri et al., 2012a).
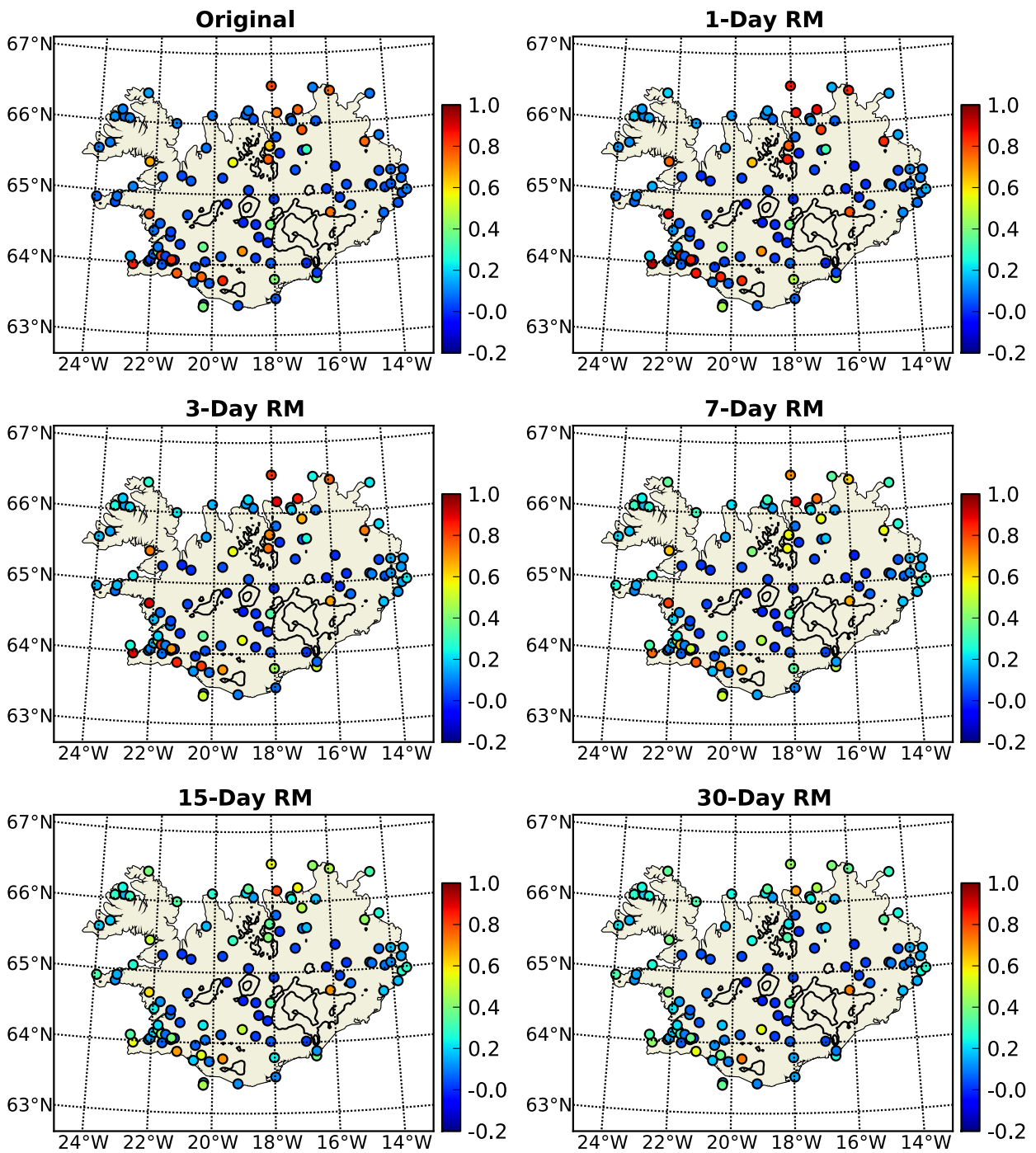
Figure 17. Correlation between WRF model and measured surface wind speeds, with 3-hourly time-series smoothed by running means over different time-periods.
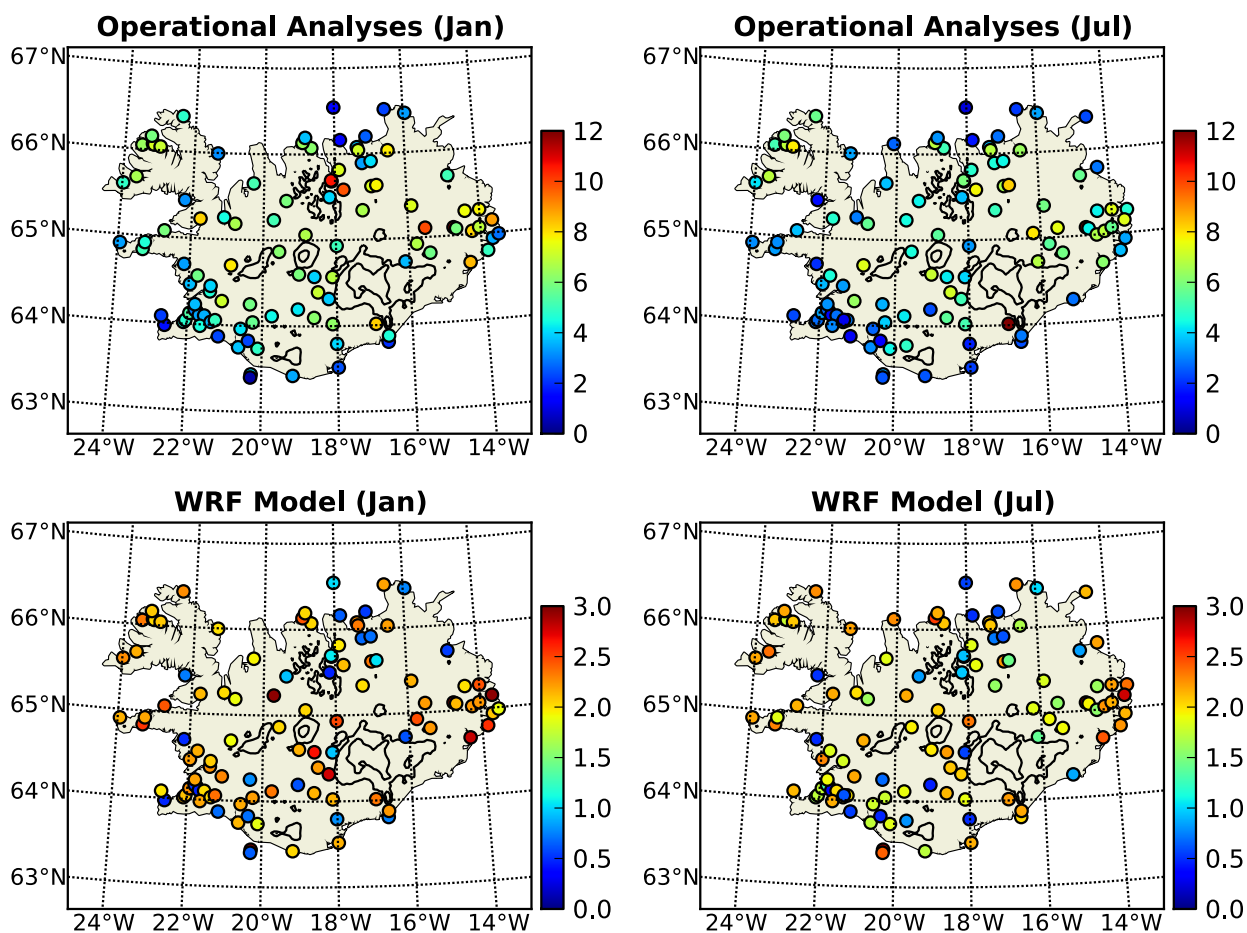
Figure 18. Normalised mean squared deviation between modelled and measured surface wind speeds.

As shown in Figure 18, different station locations are not as clearly divided into high- and low-NMSD sites as for correlation, based on the original 3-hourly time-series. However, for WRF surface wind speeds, high-correlation sites do stand out as having the lowest NMSDs. As discussed in Nawri et al. (2012b), at other locations, NMSD can be reduced to the minimum value given by (8) through a linear transformation, whereby local averages and standard deviations are made equal to the measured values.

8   Temporal Variability

It was shown in the previous section, that the temporal variability of measured surface wind speeds at most station locations is poorly represented by WRF model simulations, for which temporal fluctuations are primarily driven by the boundary-conditions determined by ECMWF operational analyses. In this section, this issue is discussed from a different point of view, by comparing the power spectra of 3-hourly measured and modelled surface wind speeds.

Figure 19. Spectral components of the annual and daily cycles of surface wind speed at station locations in percent of the total variance.
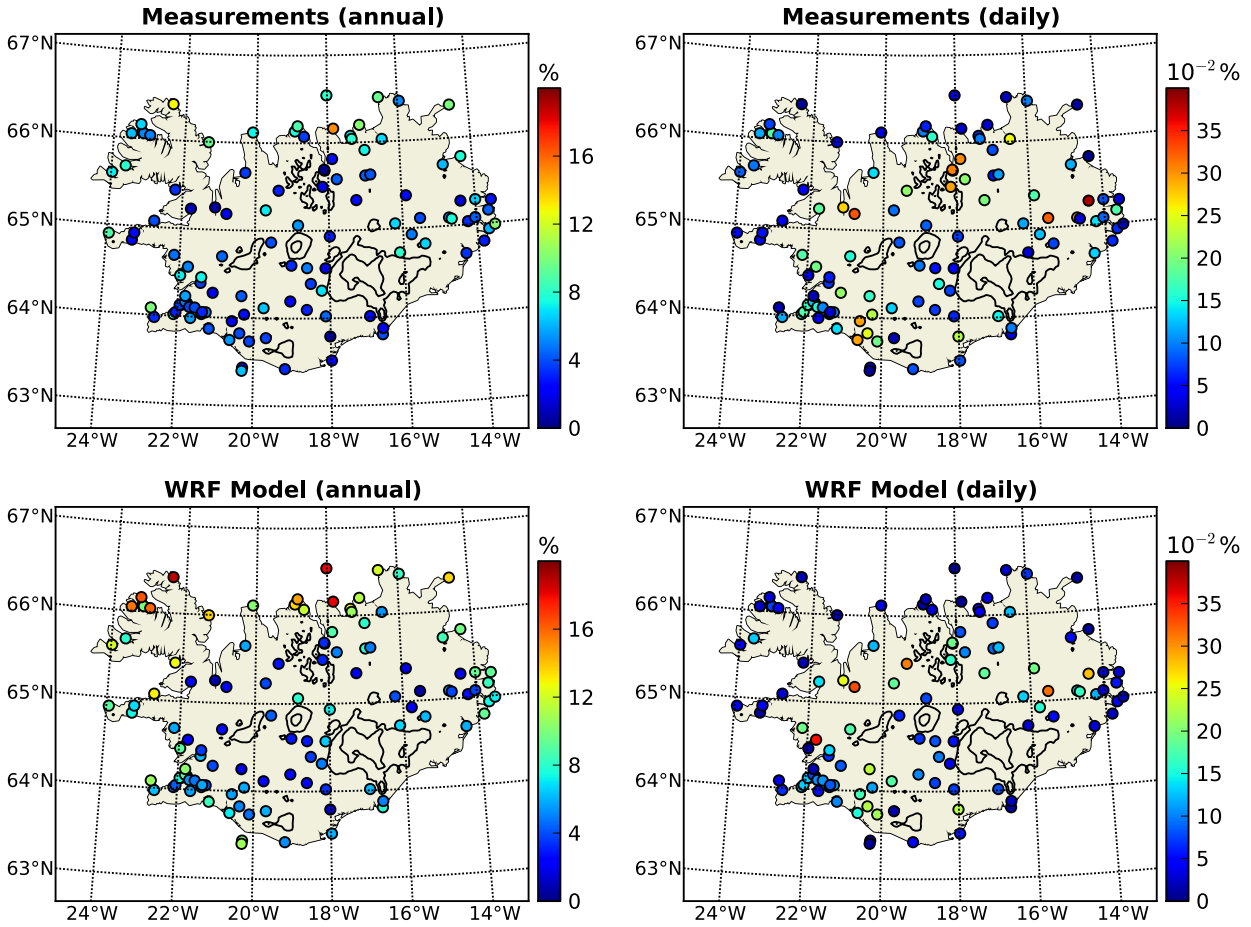
For a Fourier series representation of any discrete time-series with N data points and expansion coefficients a_n and b_n, the power spectrum consists of individual spectral components $S(\omega_n) = \left(a_n^2 + b_n^2\right)/2$, corresponding to angular frequencies $\omega_n = 2\pi n/N$, with $1 \leq n \leq (N-1)/2$. Prior to the calculation of Fourier components, gaps in measured station data are filled by linear interpolation. All time-series are detrended by subtracting the linear least squares polynomial fit. The variance of the detrended time-series is equal to the sum of all spectral components. To be able to compare the relative variability on different time-scales between different locations, all local power spectra are normalised by the total variance.

A comparison of local annual and daily normalised spectral components between modelled and measured time-series of surface wind speed is shown in Figure 19. In terms of relative temporal variability, the WRF model has stronger annual cycles primarily along the north coast, and to a lesser extent at other coastal locations, compared with measurements. Relative diurnal cycles, with the exception of a few locations, tend to be weaker in the WRF model time-series, than in measurements.

Differences between WRF and measured ensemble mean spectra for either low- or high-correlation sites are shown in Figure 20 (a), whereby low-correlation sites are defined as those with non-negative annual correlations of less than 0.5 (82% of all stations with adequate wind speed data), and high-correlation sites are defined as those with correlations of at least 0.5. For high-correlation sites, the magnitude of deviations is larger than at low-correlation sites for the lowest frequency of 0.25 cycles per year, as well as for the annual cycle. For most other frequencies, differences at high-correlation sites are smaller. Correlation between modelled and measured time-series is therefore primarily affected by fluctuations on time-scales shorter than the annual cycle.

Differences between high- and low-correlation ensemble mean spectra for either measured or modelled time-series are shown in Figure 20 (b). Differences for modelled time-series are generally smaller than those based on measurements. The main exception is the significantly larger annual cycle of modelled time-series at high-correlation sites, compared with that at low-correlation sites. At higher frequencies, the large differences in correlation between nearby locations are mainly due to differences in measured time-series. For these, particularly large differences exist at the lowest frequency, as well as around 20 cycles per year, corresponding to periods of about 18 days. The measured diurnal cycle is also considerably weaker at high-correlation sites. At higher frequencies, differences are negligible. Generally small differences are also found at frequencies between 200–300 cycles per year, corresponding to periods of about 1–2 days. As discussed in the previous section, this corresponds to the time-scale with the highest spatial coherence of temporal fluctuations across the island.
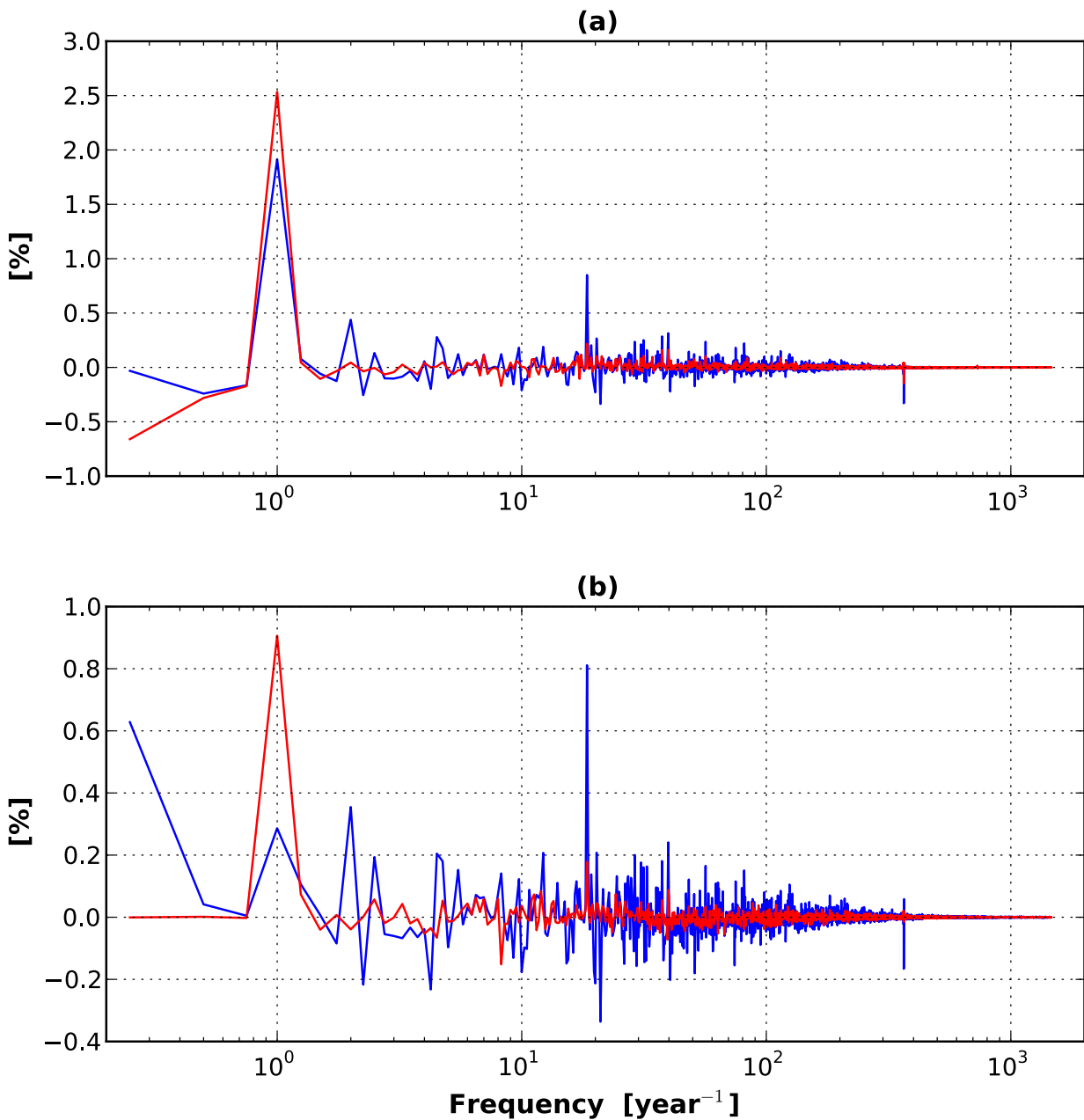
Figure 20. (a) Differences between WRF and measured ensemble mean spectra for either low-correlation sites (blue lines) or high-correlation sites (red lines). (b) Differences between high- and low-correlation ensemble mean spectra for either measured time-series (blue lines) or modelled time-series (red lines).

9 Effects of the Large-Scale Atmospheric Circulation

As demonstrated in the previous sections, as well as in Nawri et al. (2012a), under most conditions, the temporal variation of surface wind speed over Iceland is poorly correlated with the intensity of the large-scale atmospheric circulation, as determined by ECMWF operational analyses. However, the temporal variability of WRF model simulations is primarily determined by the temporal variability of operational analyses, which are used as boundary conditions. It is therefore necessary to study the performance of WRF model simulations of surface wind speeds with different large-scale conditions.

For this, the same classification of 850 hPa geostrophic wind speeds, derived from operational analyses, is used as that introduced in Nawri et al. (2012a), i.e., geostrophic wind speeds are separated into three classes, with limits at the monthly 30th and 65th percentiles. Additionally, for intermediate and strong geostrophic wind speeds, geostrophic wind directions here are also separated into four 90-degree sectors, centred around the intercardinal directions. Geostrophic wind speed is calculated from the average magnitude of the geopotential height gradient over the land area of Iceland, while the geostrophic wind direction is defined as the direction of the average of all unit vectors pointing into the direction of the geostrophic wind at each grid point. For the calculation of prevailing geostrophic wind directions, geostrophic wind speeds of less than 1 m s^{-1} are excluded.

Histograms of geostrophic wind speed and direction at 850 hPa, in comparison with the surface wind from ECMWF operational analyses, are shown in Figure 21. The wind direction probability distribution at both levels is bimodal (see Figure 21(a)). However, there is a shift from the north-northeasterly dominant surface wind direction to the south-southwesterly dominant (geostrophic) wind direction at 850 hPa. The secondary wind direction changes from southerly to northeasterly. This is indicative of an adjustment of the low-level wind from the cyclonic circulation of low-pressure systems passing primarily to the south of Iceland, to the prevailing zonal circulation aloft, associated with the polar front. At 850 hPa, south-southwesterly geostrophic wind directions occur more frequently with increasing wind speeds, indicating the relative significance of the unperturbed jet stream, compared with cyclonic weather systems, for the forcing of strong winds at low levels of the free atmosphere (see Figure 21(b)). With increasing height, from the surface to 850 hPa, the occurrence of wind speeds ≥ 10 m s^{-1} increases significantly (see Figure 21(c)).

Average monthly WRF model fields of surface wind speed for weak geostrophic wind conditions at 850 hPa are shown in Figure 22. With the exception of the summer months, relatively stronger wind speeds exist along the coast, especially in the Westfjords, than for the monthly fields shown in Figure 6, taking into account all geostrophic wind conditions.

Differences of these monthly fields from the one-parameter terrain model (Nawri et al., 2012a), projected onto the WRF model orography, are shown in Figure 23. The negative bias in the interior of the island, shown in Figure 6 for all geostrophic wind conditions, is enhanced by about a factor of two for weak geostrophic winds. Consistent with the findings in previous sections, this suggests that, in the absence of significant large-scale forcing imposed at the domain boundaries, the WRF model lacks internal forcing over the land area.
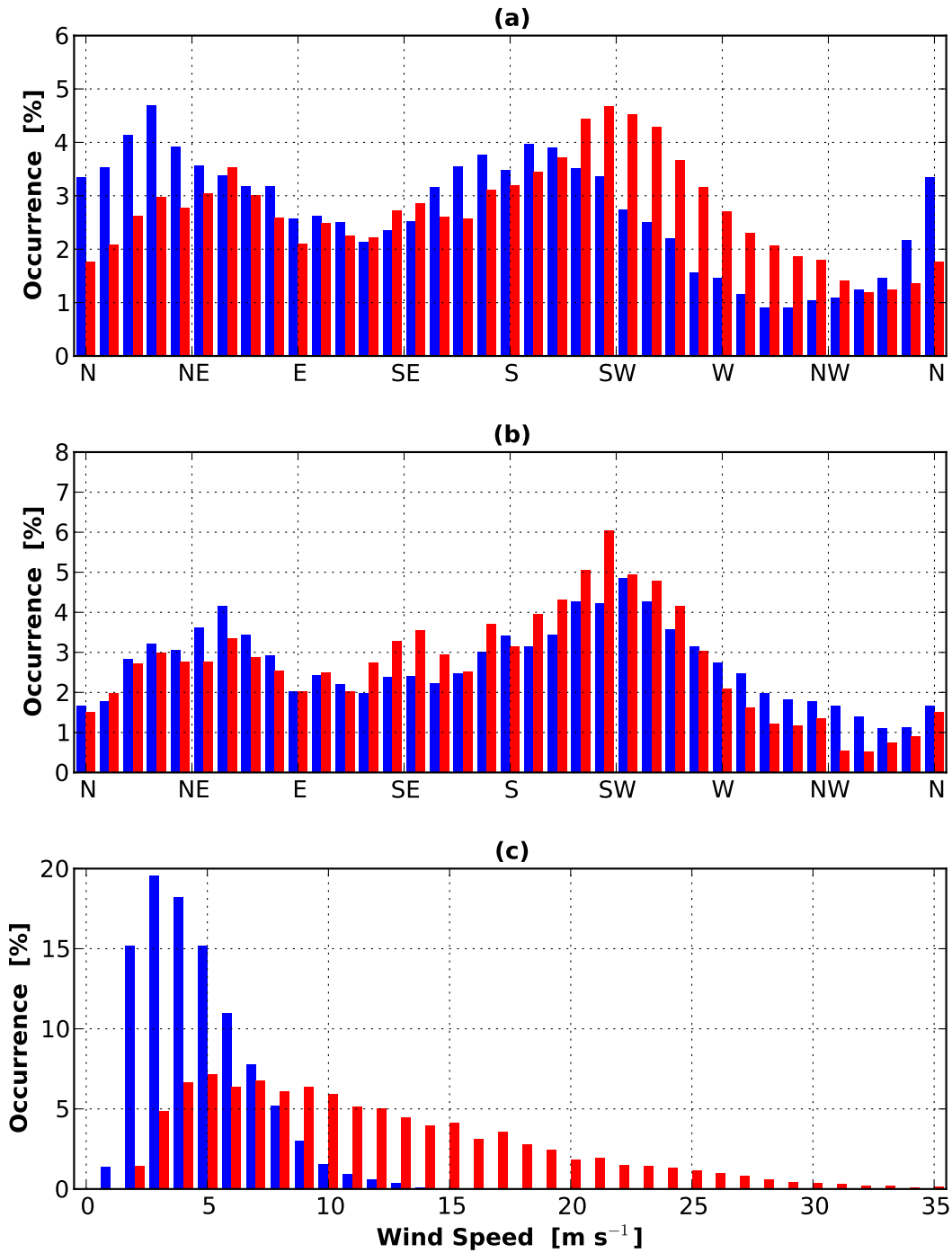
Figure 21. Histograms of prevailing wind conditions over Iceland: (a) surface wind direction (blue bars) and geostrophic wind direction at 850 hPa (red bars), for speeds of at least 1 m s^{-1}; (b) geostrophic wind direction at 850 hPa for weak (blue bars) and strong (red bars) geostrophic wind speeds; (c) surface wind speed (blue bars) and geostrophic wind speed at 850 hPa (red bars) (see Section 9 for a definition of different geostrophic wind conditions).

Figure 22. Mean monthly surface wind speed from WRF model simulations, under conditions of weak geostrophic winds (see Section 9).

Figure 23. Differences in mean monthly surface wind speed between empirical terrain models and WRF model simulations, under conditions of weak geostrophic winds (see Section 9).

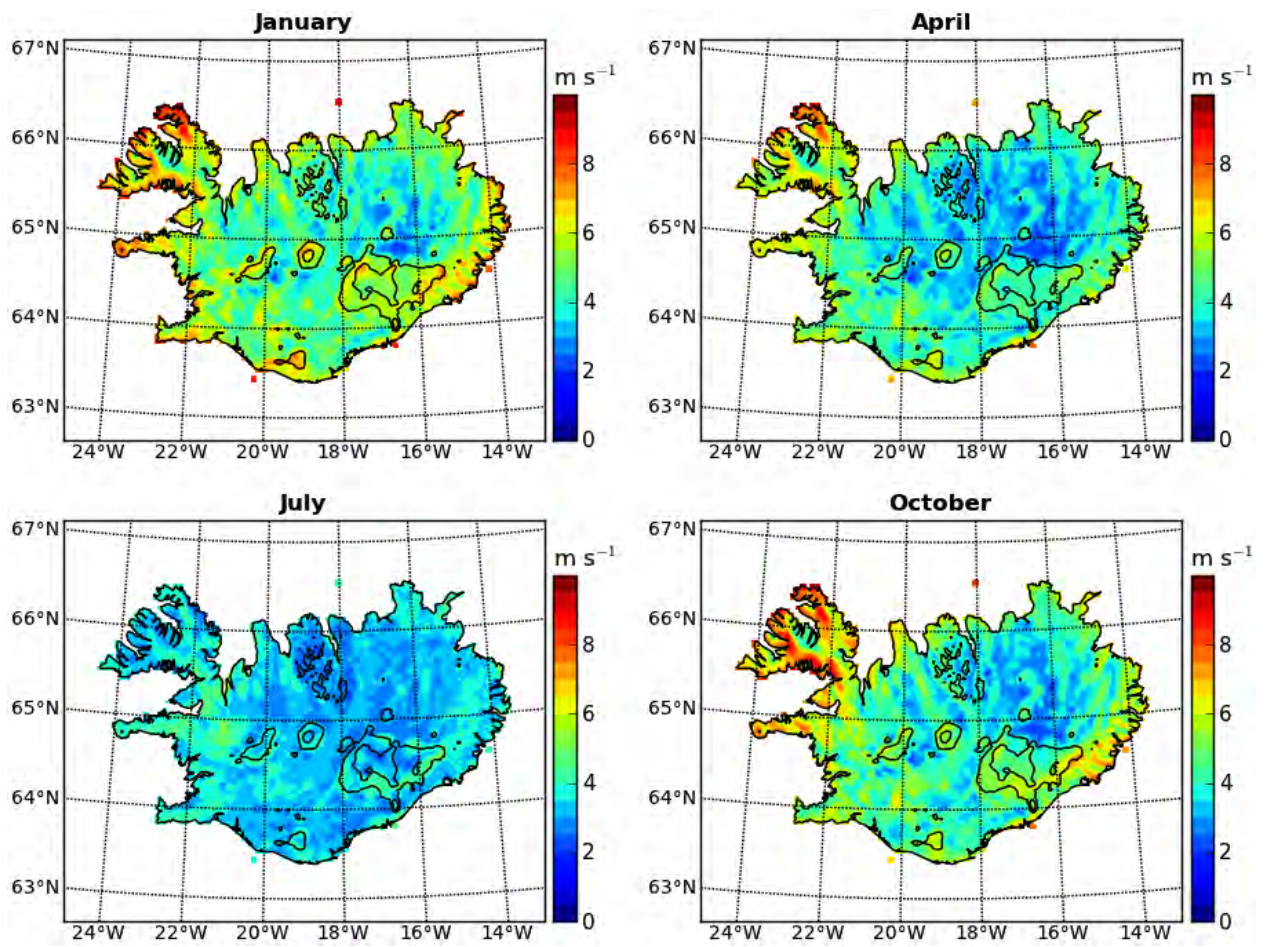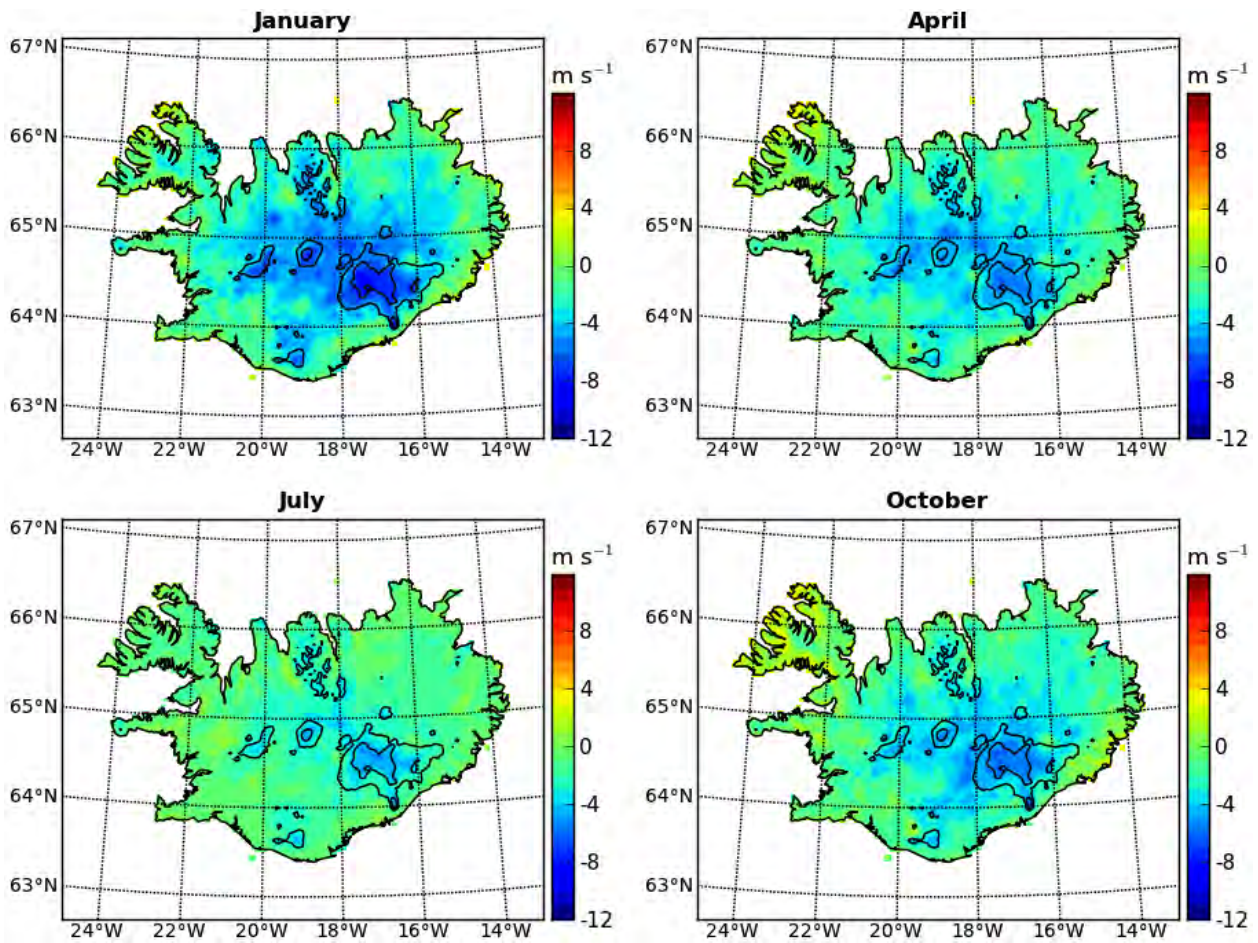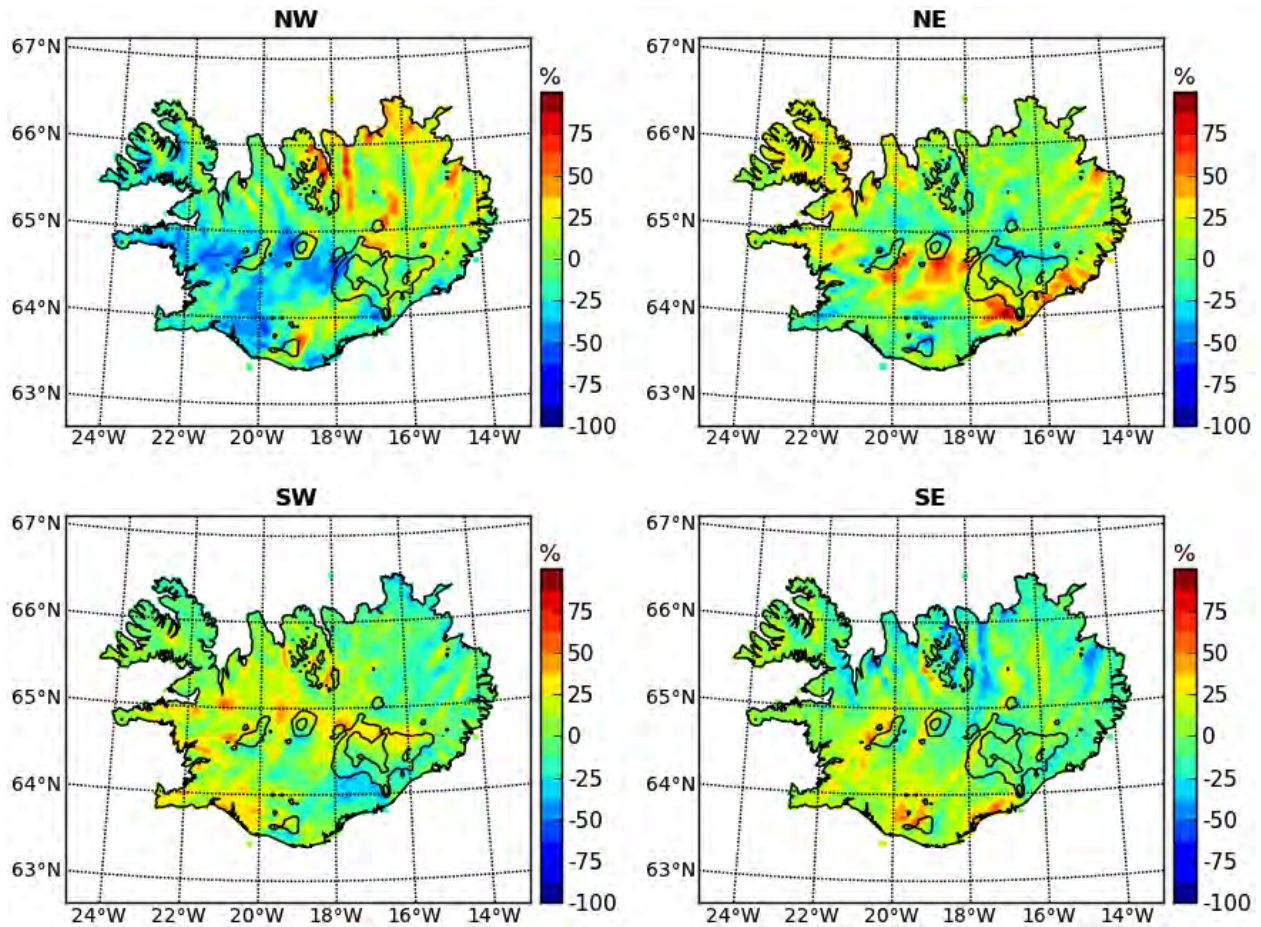*Figure 24. Anomalies of normalised surface wind speed for different geostrophic wind directions, under conditions of strong geostrophic winds in January (see Section 9).*

The effects of geostrophic wind direction on modelled surface wind speed over Iceland are determined by analysing deviations of monthly mean WRF fields for individual sectors of geostrophic wind direction from the average of the fields for all sectors. For strong geostrophic winds in January, differences of average wind speeds for individual sectors from the average for all sectors, normalised by the average field, are shown in Figure 24. There is a clear pattern of positive and negative differences for individual geostrophic wind directions, with the largest positive deviations occurring on the upper parts of lee slopes, as well as on the low-pressure side (left, facing downstream) of elevated terrain. Conversely, especially with northwesterly geostrophic winds, low-wind stagnation points are located on the lower parts of windward slopes of the three largest glaciers. For strong geostrophic winds in July, the basic pattern of normalised differences is the same as in winter, with the strongest winds occurring on low-pressure and lee slopes (not shown). Similar patterns of anomalies, although less well developed, are also found with intermediate geostrophic wind speeds (not shown).

Deviations of monthly mean WRF fields for individual sectors of geostrophic wind direction from corresponding fields of the one-parameter terrain model for strong geostrophic winds in January are shown in Figure 25. Differences are normalised by the terrain model wind speeds. As discussed in Section 4, regardless of geostrophic wind conditions, WRF surface winds tend to be too
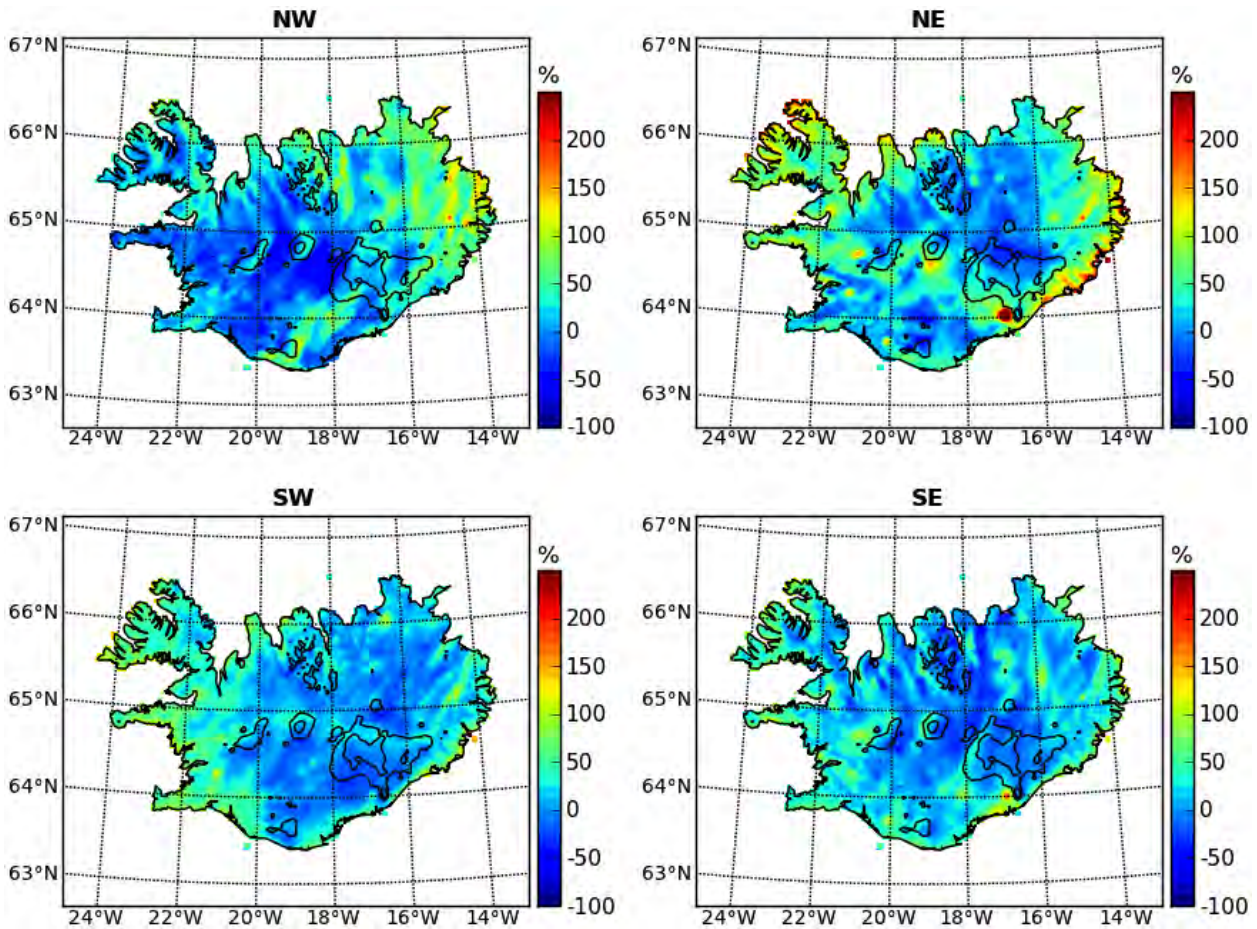
Figure 25. Differences in normalised surface wind speed between the WRF model and the one-parameter terrain model for different geostrophic wind directions, under conditions of strong geostrophic winds in January (see Section 9).

strong near the coast, and too weak in the interior. Taking into account different geostrophic wind directions in the presence of strong pressure gradients, superimposed on this basic spatial bias is a pattern of relatively high WRF wind speeds on lee and low-pressure slopes. In the terrain models, dynamical effects of flow over and around elevated terrain is not explicitly parameterised. Without sufficient coverage by local measurements, these effects are therefore not included in the terrain model. However, given the evidence from previous research, the modelled terrain effects, with respect to the model orography, may at least be qualitatively accurate.

Using atmospheric and wind tunnel measurements, as well as numerical simulations, studies of wind flow over elevated terrain under neutral or near neutral stratification (e.g., Walmsley and Taylor, 1996; Apsley and Castro, 1997; Takahashia et al., 2002, 2005; Corbett et al., 2008; Lewis et al., 2008; Moreira et al., 2012) have consistently shown a reduction of wind speed at the bottom of windward slopes, and a rapid increase towards the summit. The highest wind speeds and low-level jets are found on the crest, with a rapid decrease to below upwind speed on the lee side. Under conditions of stable stratification, field studies have shown that the highest wind speeds are shifted downstream from the summit to the uppermost part of the lee slope, with flow separation and return circulation occurring on the lower part (Vosper et al., 2002; Barkwith and Collier, 2011). Based

40

on wind tunnel measurements, Ayotte and Hughes (2004) showed that also in neutrally stratified flow the wind speed on the upper lee side increases with increased slope. Given these results, and considering the generally stable boundary-layer stratification and prevalence of steep slopes throughout Iceland, the intensification of WRF surface winds downwind from summits and ridges appears to be physically motivated. However, local measurements for direct comparisons are not available.

10   Summary

In this study, the performance of a particular setup of the WRF mesoscale model with regard to the surface wind conditions over Iceland was analysed, in comparison with local and interpolated station data. Aside from internal numerical errors and parameterised approximations, whose effects by themselves are difficult to assess, deviations of model results from measurements are due to the limited representation of the terrain, as well as the specification of atmospheric conditions at the lateral boundaries.

Terrain-related model errors are due to inaccurate representations of elevation, ruggedness, and surface roughness. Differences in elevation between model terrain and the actual height at station locations were taken into account here, either by projecting local measured or modelled values to mean sea level, or by projecting empirical terrain models onto the model orography. This is done using vertical gradients of surface wind speed over elevated terrain, based on either model fields or station data, whereby model terrain gradients are considerably smaller than those based on measurements. Furthermore, low-lying areas of the island are wrongly identified in the model as being covered with bushes and low trees. Throughout the year, with the exception of the icecaps at elevations of 1000 mASL and above, model surface roughness lengths are typically too large by up to an order of magnitude. Therefore, in addition to the small vertical terrain gradients in the WRF model, significant and systematic differences exist between model fields and interpolated measurements, with too strong surface winds along the coast, and too weak winds in the interior. The relative decrease in wind speed from the coast inland and onto the higher terrain is further enhanced by about a factor of two for weak geostrophic winds. Superimposed on this basic geographical bias is a clear pattern of positive and negative differences for individual geostrophic wind directions, with the largest positive deviations occurring on the upper parts of lee slopes, as well as along the low-pressure side of elevated terrain. Low-wind stagnation points are located on the lower parts of windward slopes of the three largest glaciers.

Previously, Bromwich et al. (2005) evaluated Polar MM5 (Version 3.5) simulations over Iceland, including surface wind speed. Polar MM5 is a specialised high-latitude version of the standard MM5 model (Grell et al., 1994), with modified cloud–radiation interaction, ice phase microphysics, turbulence parameterisation, and heat transfer through snow and ice surfaces (Bromwich et al., 2001). As in the case of the RÁV WRF simulations, Polar MM5 simulations were performed in three nested horizontal domains: the outer domain with 85×73 grid points spaced at 72 km (6048×5184 km), including northern Canada, as well as northern Europe; the intermediate domain with 108×121 grid points spaced at 24 km, encompassing all of Greenland, and extending east to include the Faroe Islands; and the inner domain with 85×73 grid points spaced at 8 km,

including Iceland as the only landmass. All three domains have 3/8 lower spatial resolution than the corresponding WRF model domains. However, while the extent of the inner domains is comparable, the intermediate and outer domains of the Polar MM5 simulations are considerably larger than those of the WRF, by about a factor of 5 for the outer domain. As for the WRF simulations, the Polar MM5 was forced at the lateral boundaries by ECMWF operational analyses. Compared against monthly mean time-series of surface wind speed at 70 automatic weather stations for the 1991–2000 period, the Polar MM5 biases between modelled and measured wind speeds of -2.5 – 2.9 m s^{-1} are comparable for the most part to those of the WRF simulations. Only in winter, positive wind speed biases in WRF simulations, projected to mean sea level, exceed 3 m s^{-1} at some locations near the coast.

Qualitatively, throughout most of the island, the WRF model captures the change in mean monthly flow from predominantly offshore in winter, to predominantly onshore in summer, which is shown by the interpolated measurements. However, in the southwest region the flow reversal is underestimated, partly due to weak wintertime offshore winds, and continued summertime downslope flow from the central highland.

The spread of modelled relative to measured surface wind speeds, expressed through the standard deviation of differences, is similar to the corresponding spread of surface wind speeds interpolated from ECMWF operational analyses. This is the result of a high temporal correlation between WRF and ECMWF surface winds. Despite differences in monthly averages, temporal fluctuations around average values in the WRF model simulations are primarily driven by the boundary conditions, rather than internal model dynamics. The lack of internal forcing is also shown by the increased negative bias over the land in the absence of significant large-scale forcing imposed at the domain boundaries. However, the dynamics creating temporal fluctuations in measured wind speeds, which are essentially disconnected from those of ECMWF winds at the model boundaries, are neither purely local, nor related to diurnal cycles such as thermal wind systems and atmospheric tides. The coherent forcing, which is not properly captured by operational analyses at the model boundaries, is active primarily on a time-scale of 1 day, while local correlations between WRF model and measured surface wind speeds are highest on a time-scale of 3 days, i.e., on time-scales of the evolution of individual cyclonic weather systems.

The RÁV WRF model representation of temporal variability on time-scales of several days and up to one month is inferior to that on shorter time-scales, as well as in comparison with the Polar MM5. The local correlation coefficients for monthly time-series of wind speed based on measurements and Polar MM5 simulations vary between 0.48 and 0.94, with an average value for all stations of 0.76 (Bromwich et al., 2005). Correlation coefficients for monthly time-series of wind speed based on measurements and WRF simulations (not shown) vary between -0.06 and 0.96, with an average value of 0.57. The corresponding correlation coefficients for the interpolated ECMWF operational analyses are similar, varying between 0.10 and 0.96, around an average value of 0.52. Local correlations between monthly time-series of wind speed based on measurements and WRF simulations are generally higher than for the 3-hourly time-series, smoothed by 30-day running means, but lower than those for the Polar MM5 simulations. Although the study by Bromwich et al. (2005) covered a different time period, both it and the RÁV WRF simulations used the same type of boundary data. The difference in performance when representing monthly variability of surface wind speed is therefore possibly due to a better representation of the atmospheric circu-

lation over the larger domain of the Polar MM5. In fact, based on the case study of a downslope windstorm in southern Iceland, Rögnvaldsson et al. (2011b) showed that with similar model setups and the same boundary conditions, the WRF model (Version 2.2) and the MM5 (Version 3.7.3) obtained results with comparable accuracy.

In short, the problems of the WRF model with reproducing temporal variability on time-scales of less than 3 days may be due to internal model dynamics, and might be improved with higher spatial resolution. In contrast, on time-scales of several days and longer, the problems with reproducing temporal variability may be related to the specific RÁV setup of the WRF model, and possibly be the result of too small intermediate and outer model domains. On these longer time-scales, increased spatial resolution is unlikely to result in improvements.

References

Apsley, D. D. and Castro, I. P. (1997). Flow and dispersion over hills: Comparison between numerical predictions and experimental data. *J. Wind Eng. Ind. Aerodyn.*, 67&68:375–386.

Ayotte, K. W. and Hughes, D. E. (2004). Observations of boundary-layer wind-tunnel flow over isolated ridges of varying steepness and roughness. *Boundary-Layer Meteorol.*, 112:525–556.

Barkwith, A. and Collier, C. G. (2011). Lidar observations of flow variability over complex terrain. *Meteorol. Appl.*, 18:372–382.

Bromwich, D. H., Bai, L., and Bjarnason, G. G. (2005). High-resolution regional climate simulations over Iceland using Polar MM5. *Mon. Wea. Rev.*, 133:3527–3547.

Bromwich, D. H., Cassano, J. J., Klein, T., Heinemann, G., Hines, K. M., Steffen, K., and Box, J. E. (2001). Mesoscale modeling of katabatic winds over Greenland with the Polar MM5. *Mon. Wea. Rev.*, 129:2290–2309.

Corbett, J.-F., Ott, S., and Landberg, L. (2008). A mixed spectral-integration model for neutral mean wind flow over hills. *Boundary-Layer Meteorol.*, 128:229–254.

Einarsson, M. Á. (1984). Chapter 7: Climate of iceland. In van Loon, H., editor, *Climates of the Oceans*, volume 15 of *World Survey of Climatology*, pages 673–697, Amsterdam, Netherlands. Elsevier.

Grell, G. A., Dudhia, J., and Stauffer, D. R. (1994). A description of the fifth-generation Penn State / NCAR Mesoscale Model (MM5). NCAR Technical Note NCAR/TN-398+STR, National Center for Atmospheric Research, Boulder, Colorado, USA.

Lewis, H. W., Mobbs, S. D., and Lehning, M. (2008). Observations of cross-ridge flows across steep terrain. *Q. J. R. Meteorol. Soc.*, 134:801–816.

Moreira, G. A. A., dos Santos, A. A. C., do Nascimento, C. A. M., and Valle, R. M. (2012). Numerical study of the neutral atmospheric boundary layer over complex terrain. *Boundary-Layer Meteorol.*, 143:393–407.

Nawri, N., Björnsson, H., Jónasson, K., and Petersen, G. N. (2012a). Empirical terrain models for surface wind and air temperature over Iceland. Report VÍ 2012-009, Icelandic Meteorological Office, Reykjavik, Iceland.

Nawri, N., Björnsson, H., Jónasson, K., and Petersen, G. N. (2012b). Statistical correction of WRF mesoscale model simulations of surface wind over Iceland based on station data. Report VÍ 2012-011, Icelandic Meteorological Office, Reykjavik, Iceland.

Nawri, N., Björnsson, H., Jónasson, K., and Petersen, G. N. (2012c). Surface wind and air temperature over Iceland based on station records and ECMWF Operational Analyses. Report VÍ 2012-008, Icelandic Meteorological Office, Reykjavik, Iceland.

Rögnvaldsson, Ó., Ágústsson, H., Einarsson, E. M., Ólafsson, H., Björnsson, H., and Sveinsson, Ó. G. B. (2007). Stöðuskýrsla vegna fyrsta árs RÁV verkefnisins. Technical report, Reiknistofa í veðurfræði, Reykjavik, Iceland.

Rögnvaldsson, Ó., Ágústsson, H., and Ólafsson, H. (2011a). Aflræn niðurkvörðun veðurs innan LOKS verkefnisins. Technical report, Reiknistofa í veðurfræði, Reykjavik, Iceland.

Rögnvaldsson, Ó., Bao, J.-W., Ágústsson, H., and Ólafsson, H. (2011b). Downslope windstorm in Iceland – WRF/MM5 model comparison. *Atmos. Chem. Phys.*, 11:103–120.

Skamarock, W. C., Klemp, J. B., Dudhia, J., Gill, D. O., Barker, D. M., Duda, M. G., Huang, X.-Y., Wang, W., and Powers, J. G. (2008). A description of the Advanced Research WRF Version 3. NCAR Technical Note NCAR/TN-475+STR, National Center for Atmospheric Research, Boulder, Colorado, USA.

Takahashia, T., Katoa, S., Murakamib, S., Ookaa, R., Yassinc, M. F., and Kono, R. (2005). Wind tunnel tests of effects of atmospheric stability on turbulent flow over a three-dimensional hill. *J. Wind Eng. Ind. Aerodyn.*, 93:155–169.

Takahashia, T., Ohtsua, T., Yassina, M., Katoa, S., and Murakami, S. (2002). Turbulence characteristics of wind over a hill with a rough surface. *J. Wind Eng. Ind. Aerodyn.*, 90:1697–1706.

Troen, I. and Petersen, E. L. (1989). *European Wind Atlas*. Risø National Laboratory, Roskilde, Denmark.

Vosper, S. B., Mobbs, S. D., and Gardiner, B. A. (2002). Measurements of the near-surface flow over a hill. *Q. J. R. Meteorol. Soc.*, 128:2257–2280.

Walmsley, J. L. and Taylor, P. A. (1996). Boundary-layer flow over topography: Impacts of the Askervein study. *Boundary-Layer Meteorol.*, 78(3-4):291–320.

WMO (2008). *Guide to Meteorological Instruments and Methods of Observation, WMO-No. 8, 7th Edition*. World Meteorological Organization, Geneva, Switzerland.